Received: 2 August 2017 | Accepted: 16 December 2017

DOI: 10.1111/jmg.12302

WILEY Journal of METAMORPHIC GEOLOGY

ORIGINAL ARTICLE

Kinetic control of staurolite–Al_2SiO_5 mineral assemblages: Implications for Barrovian and Buchan metamorphism

David R. M. Pattison[1] | **Frank S. Spear**[2]

[1]Department of Geoscience, University of Calgary, Calgary, AB, Canada

[2]Department of Earth and Environmental Sciences, Rensselaer Polytechnic Institute, Troy, NY, USA

Correspondence
David R. M. Pattison, Department of Geoscience, University of Calgary, Calgary, AB, Canada.
Email: pattison@ucalgary.ca

Funding information
Natural Sciences and Engineering Research Council of Canada, Grant Number 037233; National Science Foundation, Grant Number 1447468.

Handling Editor: Michael Brown

Abstract

The distribution and textural features of staurolite–Al_2SiO_5 mineral assemblages do not agree with predictions of current equilibrium phase diagrams. In contrast to abundant examples of Barrovian staurolite–kyanite–sillimanite sequences and Buchan-type staurolite–andalusite–sillimanite sequences, there are few examples of staurolite–sillimanite sequences with neither kyanite nor andalusite anywhere in the sequence, despite the wide (~2.5 kbar) pressure interval in which they are predicted. Textural features of staurolite–kyanite or staurolite–andalusite mineral assemblages commonly imply no reaction relationship between the two minerals, at odds with the predicted first development (in a prograde sense) of kyanite or andalusite at the expense of staurolite in current phase diagrams. In a number of prograde sequences, the incoming of staurolite and either kyanite, in Barrovian sequences, or andalusite, in Buchan-type sequences, is coincident or nearly so, rather than kyanite or andalusite developing upgrade of a significant staurolite zone as predicted. The width of zones of coexisting staurolite and either kyanite, in Barrovian sequences, or andalusite, in Buchan-type sequences, is much wider than predicted in equilibrium phase diagrams, and staurolite commonly persists upgrade until its demise in the sillimanite zone. We argue that disequilibrium processes provide the best explanation for these mismatches. We suggest that kyanite (or andalusite) may develop independently and approximately contemporaneously with staurolite by metastable chlorite-consuming reactions that occur at lower P–T conditions than the thermodynamically predicted staurolite-to-kyanite/andalusite reaction, a process that involves only modest overstepping (<15°C) of the stable chlorite-to-staurolite reaction and which is favoured, in the case of kyanite, by advantageous nucleation kinetics. If so, the pressure difference between Barrovian kyanite-bearing sequences and Buchan andalusite-bearing sequences could be ~1 kbar or less, in better agreement with the natural record. The unusual width of coexistence of staurolite and Al_2SiO_5 minerals, in particular kyanite and andalusite, can be accounted for by a combination of lack of thermodynamic driving force for conversion of staurolite to kyanite or andalusite, sluggish dissolution of staurolite, and possibly the absence of a fluid phase to catalyse reaction. This study represents an example of how kinetic controls on metamorphic mineral assemblage development have to be considered in regional as well as contact metamorphism.

KEYWORDS

Al_2SiO_5, Barrovian, Buchan, kinetics, staurolite

1 | INTRODUCTION

The petrogenesis of assemblages containing staurolite and one or more Al_2SiO_5 minerals (kyanite, andalusite and sillimanite) lies at the intersection of two research areas in metamorphic petrology: (1) the interplay between equilibrium and kinetics in controlling the mineralogy and textures of metamorphic rocks and (2) the conditions and significance of Barrovian and Buchan metamorphism. Concerning the first, a key question is the magnitude of overstepping (delay of reaction relative to equilibrium) caused by kinetic impediments to metamorphic recrystallization, and whether this significantly compromises the "equilibrium paradigm" that has dominated the interpretation of metamorphic rocks for almost a century (Carlson, Pattison, & Caddick, 2015; Spear & Pattison, 2017). Petrological evidence for significant degrees of overstepping (50–70°C), and progress of metastable reactions, has been established in contact aureoles surrounding large intrusions emplaced in the pressure range 3–4 kbar (e.g. Pattison & Tinkham, 2009; Waters & Lovegrove, 2002). In these studies, the nucleation step was interpreted to be the critical factor leading to the observed departure from equilibrium, echoing earlier inferences of Ridley and Thompson (1986) and Rubie (1998). What is more controversial is whether the same degree of overstepping occurs in regional metamorphic settings where heating rates are expected to be slower and where deformation, usually considered to reduce kinetic barriers to nucleation, may be more prevalent.

Concerning heating rate, Waters and Lovegrove (2002) noted that the time-scale of metamorphism in the aureole of the large Bushveld Complex, where they documented disequilibrium progress of reactions, approached that of regional metamorphism. Independently, studies of Barrovian regional metamorphism are increasingly finding that the time-scales of metamorphism, such as determined by high-precision "geospeedometry" and Sm/Nd garnet geochronology, is shorter than predicted by thermal models of thermal relaxation of thickened crust, on the order of a few million years (e.g. Ague & Baxter, 2007; Baxter, Ague, & DePaolo, 2002; Spear, 2014; Viete, Hermann, Lister, & Stenhouse, 2011; Viete, Oliver, Fraser, Forster, & Lister, 2013). In several of these studies, pulsed advection of heat by magmas was invoked to account for the observations, an interpretation that narrows the distinction between contact metamorphism and regional metamorphism with respect to heating rate.

Even allowing for differences in heating rate, it has been argued by several workers (Carlson et al., 2015; Gaidies, Pattison, & de Capitani, 2011; McLean, 1965; Ridley & Thompson, 1986, p. 157 and p. 159; Rubie, 1998; Waters & Lovegrove, 2002) that, because of the predicted sharp increase in nucleation rate with temperature overstep, heating rate may not be as decisive a factor in the degree of overstepping as is commonly supposed. If so, other factors, such as degree of deformation (Ridley & Thompson, 1986; Waters & Lovegrove, 2002) and availability of fluid to facilitate the mass transport required for nucleation and growth (Pattison & Tinkham, 2009; Rubie, 1986), may be of greater importance in determining the degree of disequilibrium that occurs during prograde metamorphism. Notwithstanding these considerations, there remains a fairly widespread perception that disequilibrium observed in contact metamorphism may not extend to regional metamorphism.

Concerning the second area of research, Barrovian (broadly, kyanite–sillimanite type) and Buchan (broadly, andalusite–sillimanite type) metamorphic sequences are among the most widespread metamorphic sequences in orogenic belts. In a number of orogenic belts, especially those in which intrusions are abundant, they may be closely adjacent, examples including the Dalradian of NE Scotland (Harte & Hudson, 1979), parts of New England (Albee, 1968; Thompson & Norton, 1968) and the Omineca Belt of southeastern British Columbia (Webster & Pattison, 2018). As currently interpreted in thermodynamically calculated phase diagrams (Figure 1), these two types of

FIGURE 1 Phase diagrams for metapelites calculated using the thermodynamic data described in the text, and the compositions listed in Table 1 and plotted in an AFM diagram in Figure 2. Mineral abbreviations from Kretz (1983). V=H_2O fluid (vapour). Numbered reactions correspond to those in the text. Al_2SiO_5 triple point from Pattison (1992). (a) Partial petrogenetic grid for metapelites in KFMASH (K_2O–FeO–MgO–Al_2O_3–SiO_2–H_2O). Reaction 2′ terminates in a KFASH invariant point. (b) Phase diagram for average Nelson metapelite in KFMASH. Fine dashed lines are metastable extensions of Al_2SiO_5 phase boundaries. (c) Phase diagram for average Nelson metapelite in MnNCKFMASHT (MnO–Na_2O–CaO–K_2O–FeO–MgO–Al_2O_3–SiO_2–H_2O–TiO_2). Fine dashed lines are metastable extensions of Al_2SiO_5 phase boundaries. (d) Displaced positions of reactions 2, 5 and 9 from (c) for average Nelson pelite, in which the amounts of Fe and Mg (only) have been adjusted to give whole-rock Mg/(Mg+Fe) ratios of 0.3, 0.4 and 0.5. (e) Displaced positions of reactions 2, 5 and 9 from (c) using different thermodynamic databases and *a*–*x* relations described in the text. (f) Metamorphic field gradients of Barrovian and Buchan metamorphic sequences superposed on the phase diagram of (c). The dashed line with the question marks is discussed in the text

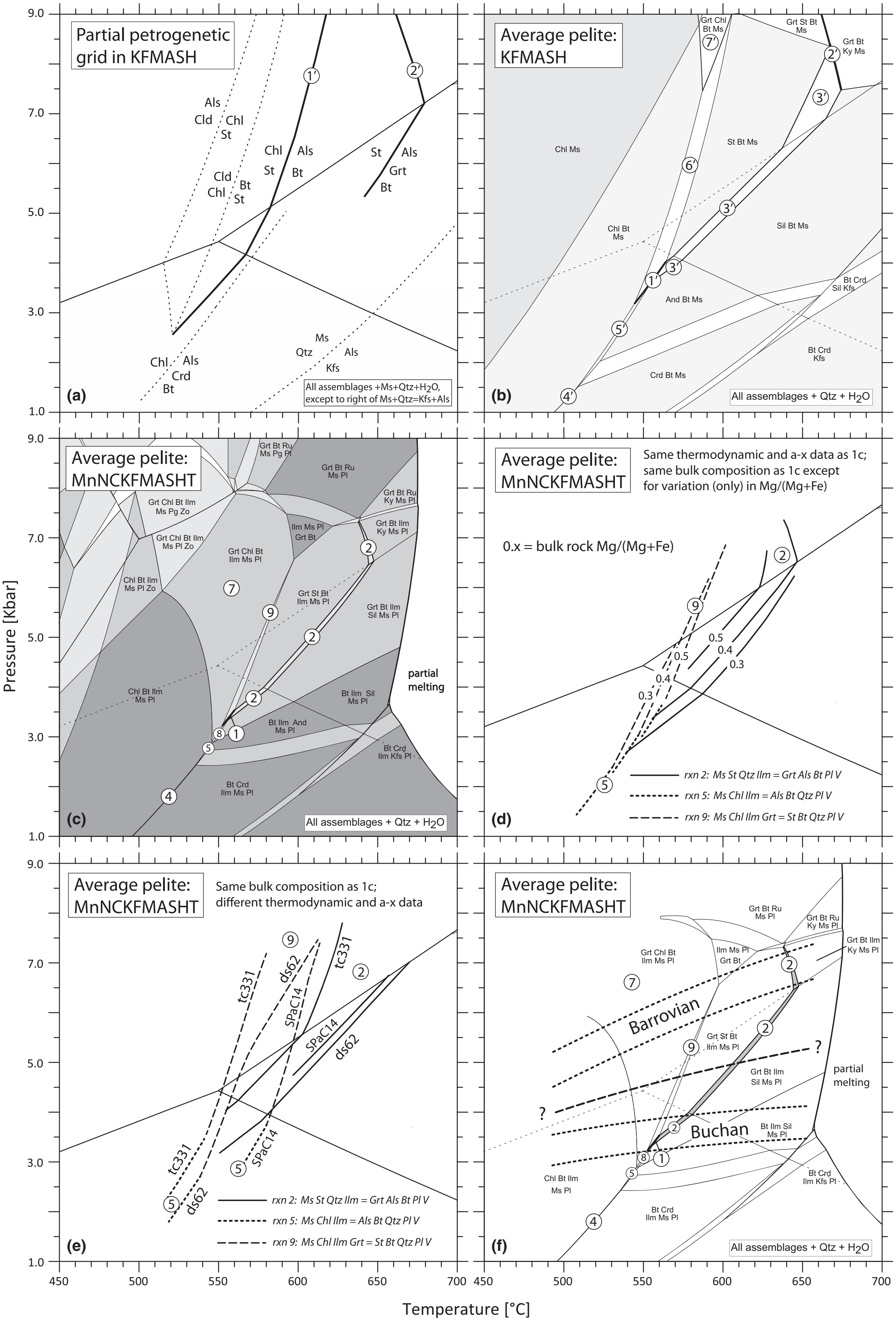
Partial petrogenetic grid in KFMASH
Als Cld Chl St
Cld Chl Bt St
Chl St Als Bt
St Grt Als Bt
1′
2′
Chl Als Crd Bt
Ms Qtz Als Kfs
All assemblages +Ms+Qtz+H$_2$O, except to right of Ms+Qtz=Kfs+Als
(a)
Average pelite: KFMASH
Grt Chl Bt Ms
Grt St Bt Ms
Grt Bt Ky Ms
7′
2′
3′
Chl Ms
St Bt Ms
6′
Chl Bt Ms
Sil Bt Ms
3′
1′
And Bt Ms
Bt Crd Sil Kfs
5′
4′
Bt Crd Kfs
Crd Bt Ms
All assemblages + Qtz + H$_2$O
(b)
Average pelite: MnNCKFMASHT
Grt Bt Ru Ms Pg Pl
Grt Bt Ru Ms Pl
Grt Chl Bt Ilm Ms Pg Zo
Grt Bt Ru Ky Ms Pl
Ilm Ms Pl Grt Bt
Grt Bt Ilm Ky Ms Pl
Grt Chl Bt Ilm Ms Pl Zo
Grt Chl Bt Ilm Ms Pl
Chl Bt Ilm Ms Pl Zo
Grt St Bt Ilm Ms Pl
Grt Bt Ilm Sil Ms Pl
partial melting
Chl Bt Ilm Ms Pl
Bt Ilm Sil Ms Pl
Bt Ilm And Ms Pl
Bt Crd Ilm Kfs Pl
Bt Crd Ilm Ms Pl
1 2 4 5 7 8 9
All assemblages + Qtz + H$_2$O
(c)
Average pelite: MnNCKFMASHT
Same thermodynamic and a-x data as 1c; same bulk composition as 1c except for variation (only) in Mg/(Mg+Fe)
0.x = bulk rock Mg/(Mg+Fe)
9
2
0.5 0.4 0.3
0.5 0.4 0.3
5
rxn 2: Ms St Qtz Ilm = Grt Als Bt Pl V
rxn 5: Ms Chl Ilm = Als Bt Qtz Pl V
rxn 9: Ms Chl Ilm Grt = St Bt Qtz Pl V
(d)
Average pelite: MnNCKFMASHT
Same bulk composition as 1c; different thermodynamic and a-x data
tc331
ds62
SPaC14
9
2
5
rxn 2: Ms St Qtz Ilm = Grt Als Bt Pl V
rxn 5: Ms Chl Ilm = Als Bt Qtz Pl V
rxn 9: Ms Chl Ilm Grt = St Bt Qtz Pl V
(e)
Average pelite: MnNCKFMASHT
Grt Bt Ru Ms Pl
Grt Bt Ru Ky Ms Pl
Grt Bt Ilm Ky Ms Pl
Grt Chl Bt Ilm Ms Pl
Ilm Ms Pl Grt Bt
7
2
Barrovian
Grt St Bt Ilm Ms Pl
9
?
Grt Bt Ilm Sil Ms Pl
partial melting
?
Buchan
Bt Ilm Sil Ms Pl
2
8
1
5
Chl Bt Ilm Ms Pl
Bt Crd Ilm Kfs Pl
Bt Crd Ilm Ms Pl
4
All assemblages + Qtz + H$_2$O
(f)
Pressure [Kbar]
1.0 3.0 5.0 7.0 9.0
Temperature [°C]
450 500 550 600 650 700

metamorphism are predicted to be markedly different in terms of P–T conditions of formation. Barrovian staurolite+kyanite-bearing assemblages are restricted to a rather high P–T range of >~630°C, >~6.5 kbar (>~23 km depth assuming a mean rock specific gravity of 2.8). Buchan staurolite+andalusite-bearing sequences, by contrast, are restricted to pressures less than ~4 kbar (<~14 km depth), leaving a large gap of ~2.5 kbar (~9 km depth) between them. Yet, there are few examples of prograde sequences whose metamorphic field gradient passes through this wide band. This anomaly is one of several in which the distribution and textures of staurolite+Al_2SiO_5 mineral assemblages do not fit with predictions of current equilibrium phase diagrams.

In this paper, we review the phase equilibria of staurolite–Al_2SiO_5 mineral assemblages, and then describe the ways in which thermodynamic predictions of these phase equilibria do not match observations from nature. We explore possible explanations for these incongruities, finding that disequilibrium processes provide the best explanation. We argue that different kinetic factors account for the various mismatches between thermodynamic prediction and observation. The paper finishes with a discussion of some of the broader implications of our findings.

2 | PHASE EQUILIBRIA OF STAUROLITE–Al_2SiO_5 MINERAL ASSEMBLAGES

Figure 1 illustrates the thermodynamically predicted phase relations of staurolite–Al_2SiO_5 mineral assemblages in metapelites. Figure 1a is a portion of a petrogenetic grid in the six-component KFMASH system (K_2O–FeO–MgO–Al_2O_3–SiO_2–H_2O), calculated using the 2003 updated version (data set ds5.5) of the Holland and Powell (1998) thermodynamic database with the activity–composition models described below. The two key univariant reactions in KFMASH that involve staurolite–Al_2SiO_5 are (abbreviations of Kretz, 1983):

$$\mathrm{Ms+Chl+St} \rightarrow \mathrm{Al_2SiO_5+Bt+Qtz+H_2O} \qquad (1')$$

$$\mathrm{Ms+St+Qtz} \rightarrow \mathrm{Grt+Al_2SiO_5+Bt+H_2O} \qquad (2')$$

Linking these two is a divariant reaction:

$$\mathrm{Ms+St+Qtz} \rightarrow \mathrm{Al_2SiO_5+Bt+H_2O} \qquad (3')$$

that is not visible in the petrogenetic grid because its stability range in most pelites is limited to intermediate values of Mg/(Mg+Fe). The use of 1′, 2′, etc., rather than 1, 2, etc., is to distinguish these KFMASH reactions from related reactions in the fuller MnNCKFMASHTO system (MnO–Na_2O–CaO–K_2O–FeO–Fe_2O_3—MgO–Al_2O_3–SiO_2–H_2O–TiO_2) that are discussed below.

The above KFMASH reactions dominated the interpretation of staurolite+Al_2SiO_5-bearing pelites from the 1960s to the 1990s (e.g. Carmichael, 1970, 1978; Guidotti, 1970, 1974; Harte & Hudson, 1979; Spear & Cheney, 1989). This situation changed with the development of thermodynamic models for phases in the fuller MnNCKFMASHTO system (e.g. Berman, 1988; Holland & Powell, 1985, 1990, 1998, 2011), and addition of the constraint of mass balance within a fixed bulk-rock composition, the latter giving rise to phase diagrams specific to individual bulk-rock compositions (Powell, Holland, & Worley, 1998).

Figure 1b,c illustrates phase diagrams calculated for an average pelite composition from the Nelson aureole, southeastern British Columbia from Pattison and Tinkham (2009). The Nelson composition is close to the average worldwide pelite composition of Ague (1991; shale/slate composition and amphibolite facies pelite composition). The Nelson composition and Ague compositions are provided in Table 1, and plotted in an AFM diagram in Figure 2, where they plot within the average "low-Al pelite" domain of Spear (1993). Two chemical systems were investigated: MnNCKFMASHT, in which C, P_2O_5 and LOI (loss on ignition) were omitted from the raw whole-rock analysis (Figure 1c); and KFMASH (system reduced from MnNCKFMASHT by projection from ilmenite, albite and anorthite and omission of MnO; Figure 1b). All Fe was treated as Fe^{2+}, in respect of the preponderance of pelites that contain ilmenite and lack hematite or magnetite, although the consequences of this assumption are examined. All mineral assemblages developed under subsolidus conditions, so excess H_2O was assumed; the suprasolidus parts of the phase diagrams in Figure 1c–f are shown as white domains labelled "partial melting".

The phase diagrams were calculated using the phase equilibrium modelling software programs THERMOCALC (Powell et al., 1998) and Theriak-Domino (de Capitani & Brown, 1987; de Capitani & Petrakakis, 2010). Where compared, Theriak-Domino reproduces the phase boundaries using THERMOCALC to within 1–2°C. The thermodynamic data set used to calculate the phase diagrams is that of Holland and Powell (1998), updated to version ds5.5. The activity–composition (a–x) relations comprise the following: garnet and chlorite—Tinkham, Zuluaga, and Stowell (2001); biotite—White, Pomroy, and Powell (2005); plagioclase—Holland and Powell (2003; ternary feldspar, Cbar1 field); white mica—Coggon and Holland (2002; margarite component omitted); ilmenite—Tinkham and Ghent (2005; ideal ternary); melt—White, Powell, and Holland (2007); all other phases including H_2O—Holland and Powell (1998). The effects of using different

TABLE 1 Whole-rock compositions used for phase diagram modelling

	Avg. pelite Nelson[a] MnNCKFMASHT	Avg. pelite Nelson[a] KFMASH	Avg. Ague pelite Shale/slate[b] MnNCKFMASHT	Avg. Ague pelite amphib facies[b] MnNCKFMASHT
wt% oxides				
SiO_2	60.41		60.34	56.25
TiO_2	0.93		0.76	1.05
Al_2O_3	20.10		17.05	20.18
FeO[c]	5.68		6.62	8.37
MnO	0.08		0.09	0.18
MgO	2.30		2.69	3.23
CaO	1.06		1.45	1.54
Na_2O	1.53		1.55	1.80
K_2O	4.17		3.64	4.02
Anhydrous total	96.26		94.19	96.62
Moles elements × 100 (after projections described in text)				
Si	100.545	81.987	100.424	93.617
Ti	1.168	—	0.952	1.315
Al	39.425	30.709	33.444	39.584
Fe^{2+}[c]	7.818	6.650	9.218	11.644
Mn	0.118	—	0.127	0.254
Mg	5.700	5.700	6.674	8.014
Ca	1.900	—	2.586	2.746
Na	4.921	—	5.002	5.808
K	8.852	8.852	7.729	8.535

[a] From table 1 of Pattison and Tinkham (2009).

[b] From table 2 of Ague (1991).

[c] All Fe recalculated as Fe^{2+}.

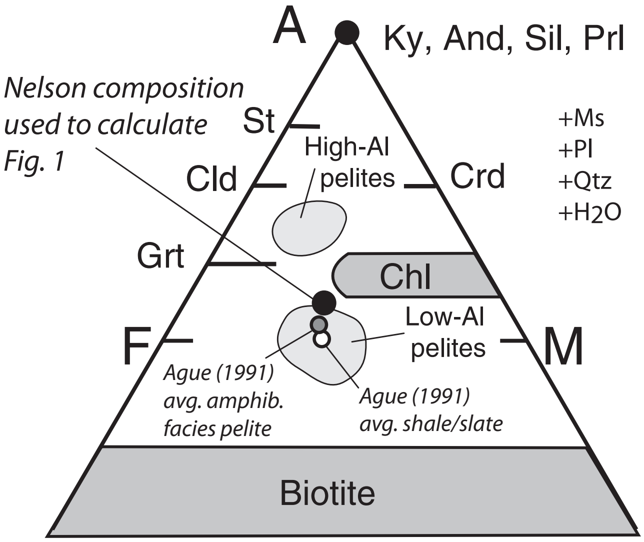

FIGURE 2 AFM diagram from Spear (1993) showing plotting positions of the average pelite compositions used to calculate Figure 1 (compositions listed in Table 1)

thermodynamic data and *a–x* relations are discussed in Section 2.1 below.

Figure 1b shows the phase diagram for average Nelson pelite in KFMASH. In addition to reactions 1′, 2′ and 3′ discussed above, other numbered reactions in Figure 1b are a series of chlorite-consuming, Fe–Mg divariant reactions, from low to high pressure:

$$\mathrm{Ms+Chl+Qtz \rightarrow Crd+Bt+H_2O} \tag{3′}$$

$$\mathrm{Ms+Chl \rightarrow Al_2SiO_5+Bt+Qtz+H_2O} \tag{4′}$$

$$\mathrm{Ms+Chl \rightarrow St+Bt+Qtz+H_2O} \tag{5′}$$

$$\mathrm{Ms+Chl+Qtz \rightarrow Grt+Bt+H_2O} \tag{6′}$$

Comparison of Figure 1a (petrogenetic grid in KFMASH) and 1b (phase diagram for average Nelson pelite in KFMASH) shows that reaction 1′ is restricted to low pressures within the andalusite stability field. This is due to the consumption of chlorite to make staurolite at higher pressure by reaction 6′, such that none is left for univariant reaction 1′ to proceed. Univariant reaction 2′ is restricted to high pressures, whereas divariant reaction 3′ traverses the andalusite, sillimanite and kyanite stability fields.

When Mn, Na, Ca and Ti are added to the model system (MnNCKFMASHT), to take account of participation of Fe–Ti oxides, plagioclase and the Ca+Mn component of garnet in the reactions, garnet stability is markedly expanded down-temperature (Figure 1c). In the MnNCKFMASHT phase diagram in Figure 1c, KFMASH reaction 1′ becomes:

$$\mathrm{Ms+Chl+St+Qtz+Ilm \rightarrow Grt+Al_2SiO_5+Bt+Pl+H_2O.} \quad (1)$$

Assignment of products and reactants for this and all other MnNCKFMASHT reactions are determined by the difference between modes on either side of the reaction, as calculated by the Theriak software (de Capitani & Brown, 1987). Reactions 2′ and 3′ from KFMASH merge into a single multivariant reaction in MnNCKFMASHT:

$$\mathrm{Ms+St+Qtz+Ilm \rightarrow Grt+Al_2SiO_5+Bt+Pl+H_2O.} \quad (2)$$

Reaction 2 traverses the andalusite, sillimanite and kyanite stability fields. Reactions 4′–7′ in KFMASH become, in MnNCKFMASHT:

$$\mathrm{Ms+Chl+Qtz+Ilm \rightarrow Crd+Bt+Pl+H_2O} \quad (4)$$

$$\mathrm{Ms+Chl+Ilm \rightarrow Al_2SiO_5+Bt+Qtz+Pl+H_2O} \quad (5)$$

$$\mathrm{Ms+Chl+Ilm \rightarrow St+Bt+Qtz+Pl+H_2O} \quad (6)$$

$$\mathrm{Ms+Chl+Pl+Ilm \rightarrow Grt+Bt+Qtz+H_2O} \quad (7)$$

Where reactions 5 and 6 extend into the garnet stability field (Figure 1c), the corresponding garnet-bearing reactions are:

$$\mathrm{Ms+Chl+Ilm \rightarrow Al_2SiO_5+Grt+Bt+Qtz+Pl+H_2O} \quad (8)$$

$$\mathrm{Ms+Chl+Ilm+Grt \rightarrow St+Bt+Qtz+Pl+H_2O} \quad (9)$$

Comparison of Figure 1b,c shows that reaction 1 in MnNCKFMASHT is restricted to even lower pressures than reaction 1′ in KFMASH because chlorite is consumed to make garnet by reaction 7 as well as staurolite by reaction 9. For pelites of normal composition in MnNCKFMASHT, reaction 1 is predicted by thermodynamics to be stable only at low pressure, within the andalusite stability field. At higher pressure, the phase equilibria of staurolite+Al_2SiO_5 assemblages is predicted to be controlled by reaction 2, with the first development of Al_2SiO_5 in a prograde sense arising from breakdown of staurolite.

2.1 | Sensitivity analysis

Sensitivity analysis was performed to see how the position of reaction 2, in MnNCKFMASHT, varies with pelite composition and with different thermodynamic data sets. In Figure 1d, the position of the lower boundary of reaction 2 (the Al_2SiO_5 mode zero-line, or Al_2SiO_5-in reaction in a prograde sense) was displaced for the most common range of whole-rock Mg/(Mg+Fe) in pelites—0.3–0.5 in increments of 0.1—by changing Mg and Fe in the average Nelson pelite composition in Table 1 to give the above ratios (with all other components unchanged). The position of reaction 2 is displaced by 10–15°C per 0.1 change in Mg/(Mg+Fe). Variations in the positions of the Al_2SiO_5 mode zero-line in reaction 5 and the staurolite mode zero-line in reaction 9 are also shown in Figure 1d for comparison.

Consideration of graphitic pelites, in which the fluid phase contains C-bearing fluid species (Connolly & Cesare, 1993), results in a displacement of reaction 2 to lower temperature by <10°C. Conversion of 15% of the total Fe in Table 1 to Fe^{3+}, well in excess of what is needed to achieve magnetite saturation, increases the effective bulk-rock Mg/(Mg+Fe) and thus results in a displacement of reaction 2 to a position that is indistinguishable from the Mg/(Mg+Fe)=0.5 position in Figure 1d. The position of reaction 2 was also calculated for the two average pelite compositions of Ague (1991) noted above, in which all Fe was treated as Fe^{2+} for consistency (Table 1). The positions of reaction 2 for both Ague compositions are displaced by <5°C compared to the Nelson position. Conversion of 15% of the total Fe in the Ague compositions to Fe^{3+} results in reaction 2 being displaced to a position that is indistinguishable from the Mg/(Mg+Fe)=0.5 position in Figure 1d.

Figure 1e shows the positions of reactions 2, 5 and 9 for the average Nelson pelite composition calculated using different thermodynamic data sets and *a–x* relations:

1. the same Holland and Powell (1998) data set as used in Figure 1c (ds5.5), but with the 2007 "Thermocalc331" *a–x* relations, labelled as "tc331" in Figure 1e: (http://www.metamorph.geo.uni-mainz.de/thermocalc/software/index.html);
2. thermodynamic data set ds6.2 of Holland and Powell (2011) and the *a–x* relations of White, Powell, Holland, Johnson, and Green (2014) and White, Powell, and Johnson (2014), labelled as "ds62" in Figure 1e; and
3. data set SPac14, a modification of the Spear and Cheney (1989) data set, described in Pattison and DeBuhr (2015, p. 457), which is labelled in Figure 1e as "SPaC14". The maximum difference is between the first two. The low-temperature positions of the reactions

using “tc331” are largely a function of the biotite *a–x* model of White et al. (2007) that was optimized for partially melted pelites. The predicted subsolidus phase equilibria using “tc331” show poorer agreement with natural constraints than the earlier *a–x* models (e.g. compare figure 13b,c of Pattison & DeBuhr, 2015). Neglecting the “tc331” position of reaction 2, the intersection of reaction 2 and the kyanite–sillimanite curve is constrained to the interval 6.5 ± 0.5 kbar and 630 ± 20°C.

2.2 | Other bulk compositions

In less common high-aluminium pelites (Figure 2), staurolite and Al_2SiO_5 minerals, especially kyanite, may develop in chlorite-bearing, biotite-free assemblages at relatively low metamorphic grade, within the regional biotite and garnet zones as defined by mineral assemblages in common pelites. These assemblages commonly additionally contain chloritoid and paragonite. Example localities include: the Shetland islands (Flinn, Key, & Khoo, 1996); northern Vermont (Albee, 1968); the Picuris region of New Mexico (Holdaway, 1978); northwestern Variscan Iberia (Reche, Martinez, Arboleya, Dietsch, & Briggs, 1998); the Lukmanier Pass, Switzerland (Fox, 1975); and the Tono aureole, Japan (Okuyama-Kusunose, 1994). Another type of unusual pelitic rock composition comprises pelites of normal Al content but which are either strongly oxidized (as indicated by the presence of hematite) or have high sulphide content, both of which result in anomalously high Mg/(Mg+Fe) ratios in silicate phases (e.g. Thompson, 1972). These bulk compositions have been observed to develop staurolite-free Al_2SiO_5-bearing mineral assemblages at lower grade than in rocks of common Mg/(Mg+Fe) ratios, as for example documented in the Scottish Barrovian zones between Glens Esk and Lethnot where kyanite in staurolite-free hematite-bearing schists occurs downgrade of the “normal” kyanite zone (Harte, 1975, 1987).

Although noteworthy, these unusual rock compositions are subordinate to the more common low- to intermediate-Al rock compositions that plot below or close to the garnet-chlorite tie line in the AFM diagram, with intermediate values (0.3–0.5) of Mg/(Mg+Fe) (Figure 2). In these more common pelitic compositions, the first development of staurolite and Al_2SiO_5 minerals in a prograde sense is accompanied by the development, or further growth, of biotite from a muscovite+chlorite-bearing precursor assemblage (biotite, garnet or more rarely chloritoid may additionally be present in the precursor assemblage) (Figure 1). It is these common pelitic compositions that are the focus of this paper.

In the next sections, we compare the predictions from the phase equilibria modelling with observations of natural metamorphic sequences, as follows:

1. Global occurrence of prograde sequences involving staurolite–Al_2SiO_5 mineral assemblages.
2. Textures of staurolite–Al_2SiO_5 mineral assemblages.
3. Sequence and spacing of isograds marking the incoming of staurolite and Al_2SiO_5.
4. With of the zone of coexistence of staurolite and either kyanite and andalusite.
5. Nature of the demise of staurolite.

3 | PROGRADE SEQUENCES INVOLVING STAUROLITE–Al_2SiO_5 MINERAL ASSEMBLAGES

Metamorphic sequences containing kyanite- or staurolite+kyanite-bearing assemblages—broadly, Barrovian metamorphic sequences—are common in orogenic belts worldwide. Metamorphic settings containing staurolite+andalusite-bearing assemblages are also abundant, occurring in contact aureoles around intrusions and in low-*P* regional terranes (Pattison & Tracy, 1991). These are sometimes termed “higher-pressure Buchan” or “Type 2b” sequences, compared to “lower-pressure Buchan” or “Type 2a” sequences that contain cordierite instead of staurolite (Pattison & Tracy, 1991). Representative metamorphic field gradients corresponding to these two settings, assuming they develop according to stable reactions in the phase diagram in Figure 1c, are shown in Figure 1f. Between the two is a large domain, between ~4.0 and ~6.5 kbar, in which prograde sequences are predicted to develop staurolite+sillimanite-bearing assemblages with neither kyanite nor andalusite developed anywhere in the sequence. The absence of kyanite or andalusite anywhere in the prograde sequence is an important distinction from the many sequences worldwide that have a staurolite-bearing zone that passes upgrade into a sillimanite zone, but which contain kyanite or andalusite downgrade of the sillimanite zone (these sequences are addressed separately in Sections 6 and 7 below).

Given the large (2.5 kbar wide) pressure range of this domain, there should be many examples of such a prograde sequence. Examination of the petrological literature reveals that, in contrast, there are very few examples. One example is the chlorite-free staurolite-to-sillimanite isograd sequence north of Stonehaven, northeast Scotland (Harte, Booth, & Fettes, 1987; Harte & Hudson, 1979). Kyanite is not observed anywhere in the sequence and andalusite is restricted to rare, oxidized muscovite+andalusite+cordierite+biotite+hematite+magnetite-bearing schists in the lower part of the staurolite zone (Tilly Daff locality; D.R.M. Pattison, unpublished data). The presence of andalusite in rare Ms+Crd+And+Bt rocks implies a maximum pressure of ~4 kbar for the Stonehaven sequence according to Figure 1a (see also figure 10 of

Pattison, Spear, DeBuhr, Cheney, & Guidotti, 2002). Thus, the Stonehaven St-to-Sil sequence traverses the lowest pressure part of the aforementioned 2.5 kbar interval.

A second example is a domain in west-central Manitoba between File Lake and the town of Snow Lake (Froese & Gasparrini, 1975; Froese & Moore, 1980). At File Lake, metamorphosed turbidites host a staurolite-to-sillimanite sequence with no kyanite or andalusite developed anywhere in the sequence (Bailes & McRitchie, 1978; Briggs & Foster, 1992; Gordon, 1989; Gordon, Ghent, & Stout, 1991). A possible complication in the interpretation of the File Lake prograde sequence is the status of modally minor chlorite and muscovite, in particular whether they represent primary or secondary (retrograde) minerals (Briggs & Foster, 1992). In the vicinity of Snow Lake, the prograde sequence is the same in the metamorphosed turbidites as at File Lake, but kyanite is locally developed in metamorphosed alteration zones associated with the volcanic-exhalative ore bodies in the area (Froese & Moore, 1980). Zaleski, Froese, and Gordon (1991) demonstrated that the unusual bulk composition of the altered rocks (more magnesian and with F-bearing mica) resulted in the development of kyanite at atypically low grade, within the regional staurolite zone of the surrounding metamorphosed turbidites.

Other proposed examples of St-to-Sil sequences with neither kyanite nor andalusite developed anywhere in the sequence have features that compromise their status. In the Rangeley area of Maine, Guidotti (1974) mapped a series of isograds marking the transition from the staurolite zone to the sillimanite zone, which he attributed to progress of reaction 1′ in what he termed the M3 metamorphic event. However, this area is polymetamorphic (Guidotti, 1970; Guidotti & Holdaway, 1993; Guidotti & Johnson, 2002), with an early staurolite+andalusite assemblage (M2) that was overprinted by a later sillimanite-forming event (M3). An additional complication is that Guidotti (1974) and Guidotti, Teichmann, and Henry (1991) argued that chlorite was a reactant in the staurolite-forming reaction during the M3 event, whereas Holdaway, Dutrow, and Hinton (1988) and Holdaway and Dutrow (1989) argued that most of the chlorite in the rocks is retrograde (post-M3). A further complication is that andalusite in some areas appears to be an M3 mineral (C.T. Foster, pers. comm., 2017). In Connemara, Ireland, where Yardley, Leake, and Farrow (1980) mapped a staurolite-to-sillimanite transition, andalusite and rarely kyanite occur in a few localities below the sillimanite isograd and in many localities above it, and these authors additionally mapped an andalusite-out isograd.

Even accepting debate about some of the above interpretations, and the possible existence of other examples of which the authors are unaware, the central fact is that prograde staurolite-to-sillimanite sequences without kyanite or andalusite anywhere in the sequence are rare in the geological record, an observation that is at odds with the predictions from thermodynamics discussed in Section 2 and illustrated in Figure 1f.

4 | TEXTURES OF STAUROLITE–Al_2SiO_5 MINERAL ASSEMBLAGES

4.1 | Barrovian staurolite+kyanite-bearing assemblages

Based on the authors' experience, published accounts (e.g. Harte & Johnson, 1969; Nagel, de Capitani, & Frey, 2002; Whitney, Mechum, Kuehner, & Dilek, 1996) and the results of a web survey conducted in 2015, there are few examples of metapelitic staurolite+kyanite-bearing assemblages in which staurolite shows textural evidence of breaking down to form kyanite, whether directly or in separate domains such as described by Carmichael (1969) for staurolite breaking down to sillimanite. Most commonly, there is no evidence of any reaction relationship between staurolite and kyanite. Exceptions to this generality may occur in terranes that have been subjected to superposed metamorphic events of different P–T conditions.

An example of a possible reaction relationship is shown in the photomicrograph in Figure 3a from sample 79-149 from the Littleton Formation, Vermont (Spear & Rumble, 1986). In this sample, small anhedral inclusions of staurolite in kyanite porphyroblasts are consistent with kyanite growth at the expense of staurolite. In a sample from the Hyllestad schists of western Norway, D.J. Waters (written communication, 2017) observed textural evidence for a prograde transition between staurolite and kyanite in which staurolite is replaced by coarse random muscovite and the

FIGURE 3 Photomicrographs of metapelitic staurolite+kyanite-bearing assemblages. See text for discussion of these images. (a) Kyanite porphyroblast with anhedral inclusions of staurolite, Littleton Formation, Vermont (sample 79-149 of Spear & Rumble, 1986). (b) Cathodoluminescence image of kyanite from Mt. Grant area, central Vermont, with angular inner domain reminiscent of staurolite. Unpublished image from Horkley et al. (2013). (c) Euhedral kyanite and staurolite from near Caplongue, France. (d) Euhedral kyanite and staurolite in a muscovite–biotite–garnet schist from Kootenay Lake, British Columbia. (e) Euhedral kyanite and staurolite from the Mine aureole, British Columbia. (f) Kyanite and staurolite from the Glacier Creek aureole, British Columbia. (g) Topotaxial intergrowth between kyanite and staurolite, with both minerals surrounded and replaced at their edges by fibrous sillimanite, Glacier Creek aureole, British Columbia. (h) Intergrown kyanite and euhedral staurolite, Glen Clova, Scotland (Farber, 2011; Farber et al., 2014)

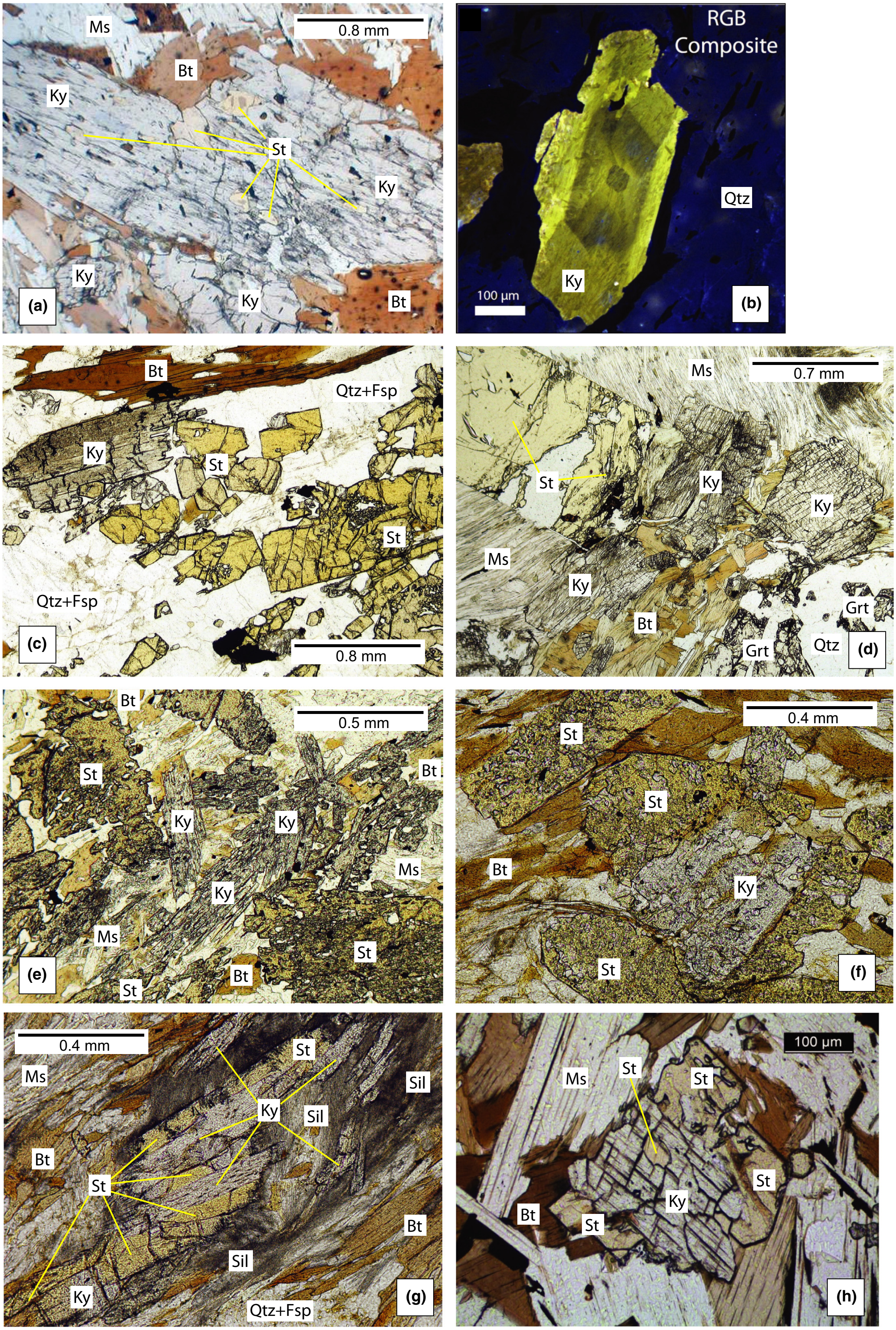
Ms
0.8 mm
Bt
Ky
St
Ky
Ky
Ky
Bt
(a)
RGB Composite
Qtz
Ky
100 µm
(b)
Bt
Qtz+Fsp
Ky
St
St
Qtz+Fsp
(c)
0.8 mm
Ms
0.7 mm
St
Ky
Ky
Ms
Ky
Bt
Grt
Grt
Qtz
(d)
Bt
0.5 mm
St
Bt
Ky
Ky
Ms
Ky
Ms
St
Bt
St
(e)
St
0.4 mm
St
Bt
Ky
St
(f)
0.4 mm
St
Ms
Sil
Ky
Sil
Bt
St
Bt
Sil
Ky
Qtz+Fsp
(g)
100 µm
Ms
St
St
Ky
St
Bt
St
(h)

kyanite grows in muscovite-rich domains elsewhere (cf. Carmichael, 1969). Figure 3b shows a cathodoluminescence image of kyanite from Mt. Grant, central Vermont (Horkley, Spear, Ruscitto, & Tailby, 2013) that contains an internal elongate, angular domain that could be interpreted as a former staurolite grain pseudomorphed by kyanite.

The above examples are exceptions to the more common situation in which staurolite and kyanite show no reaction relationship. Four examples of the latter are provided in Figure 3c–f. The samples come from respectively: the Caplongue region, France (Pattison, de Capitani, & Gaidies, 2011); Kootenay Lake Barrovian sequence, British Columbia (Moynihan & Pattison, 2013); the Mine aureole, British Columbia (Webster & Pattison, 2018); and the Glacier Creek aureole (D.R.M. Pattison, unpublished data). Photomicrographs of a garnet–staurolite–kyanite schist from the Danba culmination in East Tibet in figure 7 of Palin, Weller, Waters, and Dyck (2016) also show no evidence of a reaction relationship between staurolite and kyanite. The textural evidence suggests instead that the staurolite and kyanite porphyroblasts grew independently of each other. In their detailed studies of the staurolite and kyanite zones in the classic Barrovian sequence in Glens Esk and Clova in Scotland, Chinner (1965) and Harte and Johnson (1969) noted the substantial zone of coexistence of the two minerals yet made no mention of textural evidence for reaction of staurolite to kyanite, drawing attention instead to the textural evidence for approximately coeval development of the minerals along with garnet; McLellan (1985) mentioned "rare examples of kyanite overgrowing staurolite" in the same area, but provided no evidence.

Rocks whose individual *P–T* paths may differ from the mapped zonal sequence (metamorphic field gradient) must also be considered. In Barrovian sequences that develop a staurolite-free kyanite zone, such as at Mica Creek, British Columbia (Digel, Ghent, Carr, & Simony, 1998; Ghent et al., 1977), it is possible that these assemblages could develop along a *P–T* path that never passed through the staurolite stability field, such as one that enters the kyanite field from high pressure (Figure 1c). In this case, the reaction introducing kyanite is predicted to be approximately Grt+Ms→ Ky+Pl+Bt. The viability of this reaction to produce significant kyanite would have to be evaluated against the modal and textural features of these assemblages. Even if such a reaction were to provide an explanation for staurolite-free, kyanite-bearing assemblages and their textures, the observations concerning staurolite+kyanite-bearing mineral assemblages noted above remain.

4.1.1 | Topotaxial intergrowth of staurolite and kyanite and relation to crystallography

A special texture involving staurolite and kyanite that is sometimes observed is topotaxial intergrowth of the two minerals (Wenk, 1980 and references therein). A famous locality where this relationship is seen in hand sample is Alpe Sponda in Ticino, Switzerland (Weiss, 2014), where the two minerals occur in unusual paragonite-bearing schists located within the staurolite–kyanite zone of the eastern Lepontine Barrovian metamorphic sequence (Beiter, Wagner, & Markl, 2008; Nagel et al., 2002). An example of topotaxial intergrowth of staurolite and kyanite in thin section is shown in Figure 3g in a sample from the Glacier Creek aureole, British Columbia (D.R.M. Pattison, unpublished data), and a possible example is shown in Figure 3h in a sample from Glen Clova in the Scottish Barrovian zones (Farber, 2011; Farber, Caddick, & John, 2014). Intergrown staurolite and kyanite is anticipated, if their growth is contemporaneous, because the crystal structure of staurolite consists of Al_2SiO_5 layers with the kyanite structure alternating with AlO–OH–2FeO layers (Ferraris, Makovicky, & Merlino, 2004; figure 1 of Wenk, 1980). Intergrowth textures of staurolite and kyanite have sometimes been interpreted as a reaction relationship, such as partial replacement of staurolite by kyanite, or vice versa, but caution is merited given the above considerations. The crystallographic similarity of kyanite and staurolite carries further implications for their nucleation behaviour, as discussed in more detail in Section 9.3 below.

4.2 | Buchan-type staurolite+andalusite-bearing assemblages

Buchan-type staurolite–andalusite mineral assemblages show textures indicating andalusite growth independent of staurolite, as well as at the expense of staurolite. Figure 4a shows euhedral staurolite and andalusite crystals from the Nelson aureole, British Columbia, for which there is no indication of a reaction relationship between the two; rather, the two minerals appear to have grown independently. Figure 3a,b of Pattison and Tinkham (2009) shows other textural varieties of staurolite and andalusite from the Nelson aureole for which there is also no evidence of a reaction relationship.

It is commonly observed that staurolite is included in andalusite, but rarely if ever the reverse (Lang & Dunn, 1990; Pattison & Tinkham, 2009; Pattison & Tracy, 1991). This observation, although implying a growth time sequence, does not necessarily imply that staurolite was a reactant for andalusite. For example, Figure 4b shows a sample from the Nelson aureole in which euhedral staurolite crystals impeded the growth of andalusite (predated at least the outer margins of andalusite), yet show no evidence for consumption.

Other rocks do show evidence of replacement of staurolite by andalusite. Figure 4c shows partial replacement of small staurolite crystals by andalusite from the Scottish

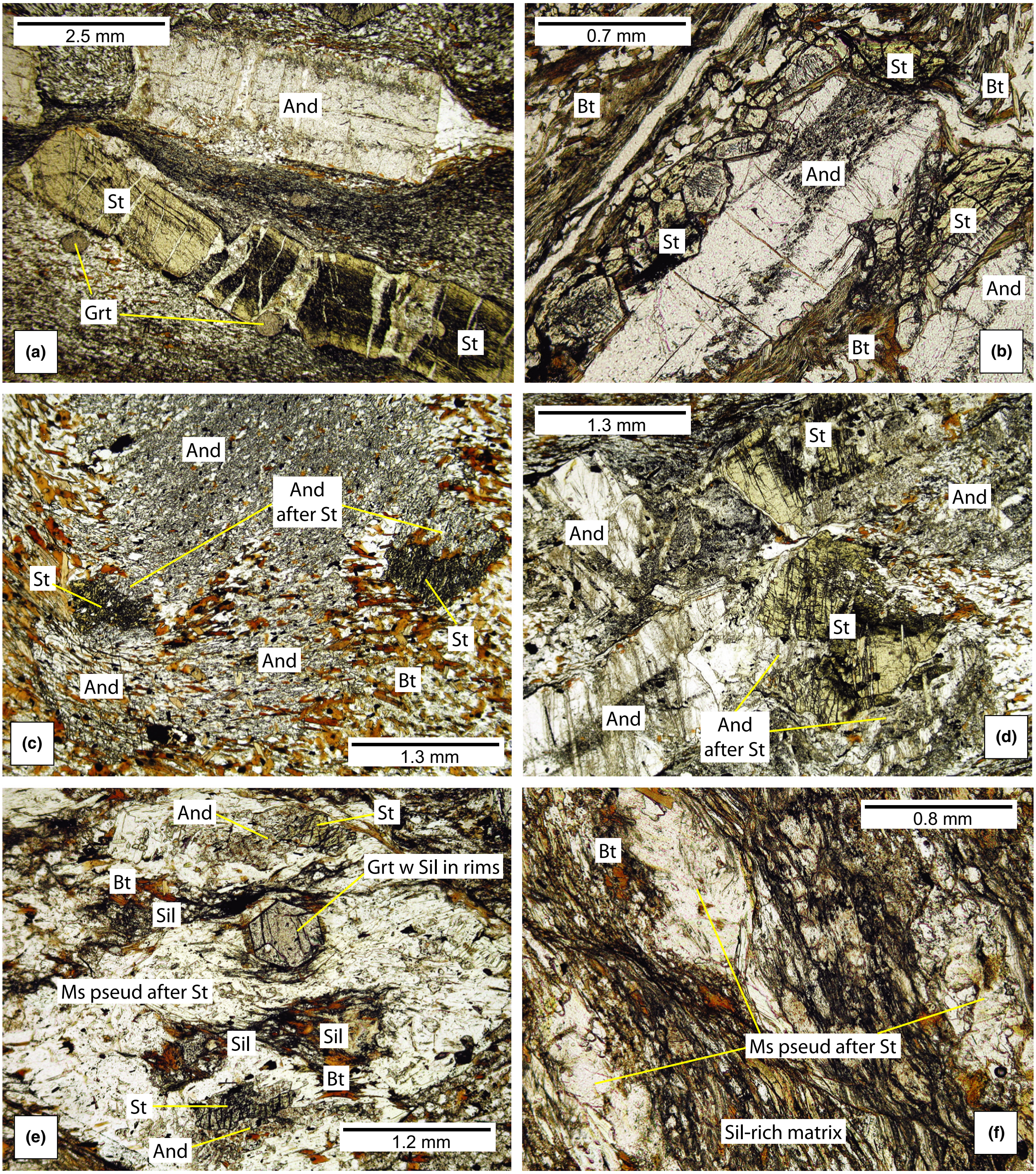

FIGURE 4 Photomicrographs of metapelitic staurolite+andalusite and staurolite+sillimanite assemblages. See text for discussion of these images. Localities in the Nelson aureole, British Columbia are from Pattison and Vogl (2005). (a) Euhedral andalusite and staurolite from Area D of the Nelson aureole. Note that the porphyroblasts have been pulled apart. (b) Euhedral staurolite partially overgrown by andalusite from Area J of the Nelson aureole. (c) Andalusite overgrowing the matrix schistosity and partially replacing two staurolite porpyhroblasts, from near Whitehills, Buchan region, Scotland. (d) Andalusite porphyroblasts, and partial replacement of staurolite by andalusite, from Area D of the Nelson aureole. (e) Muscovite-rich pseudomorph after staurolite and andalusite, with fibrous sillimanite and garnet. The garnet has inclusions of sillimanite in the rims. From Area D of the Nelson aureole. (f) Muscovite-rich pseudomorphs after staurolite in a sillimanite-rich matrix, from Area D of the Nelson aureole

Buchan coastal sequence near Whitehills, and Figure 4d shows partial replacement of staurolite by andalusite in the Nelson aureole, British Columbia. Figure 3d–f of Pattison and Tinkham (2009) from the Nelson aureole, and figures 11 and 12 of Lang and Dunn (1990) from the regional Buchan terrane near Harpswell Neck, Maine, show other examples of partial replacement of staurolite by andalusite. Garnet growth associated with the staurolite-to-andalusite reaction may sometimes be demonstrated through inclusion relationships (e.g. staurolite inclusions in garnet rims) and changes in chemical zoning (e.g., Pattison & Tinkham, 2009). Taken together, these features are consistent with the stoichiometry of reaction 2. Yet, even though these examples provide evidence for reaction of staurolite to andalusite, the modal amount of andalusite in some of the samples exceeds what can be attributed to the amount of staurolite consumption seen in the thin section (e.g. Figure 4c). In these cases, some or much of the andalusite may have grown from a different reactant that may have been completely consumed, with matrix minerals being likely candidates.

4.3 | Staurolite+sillimanite-bearing assemblages

Staurolite–sillimanite assemblages show distinct textural characteristics compared to staurolite–kyanite and staurolite–andalusite assemblages. Sillimanite does not form distinct porphyroblasts like kyanite and andalusite, occurring instead as fine grained, elongate crystals and in masses of very fine grained, fibrous sillimanite ("fibrolite") in a variety of textural varieties. These include isolated needles and small aggregations in grain boundary domains, especially those involving quartz; fibrolite-rich masses within biotite and in other isolated domains within the matrix; and anastomosing seams of sillimanite/fibrolite that transect sillimanite-free parts of the rock and bear an uncertain relationship with the rest of the minerals in the rock (e.g. Chinner, 1961; Foster, 1977, 1981, 1999; Kerrick, 1987; Pattison & DeBuhr, 2015; Vernon, 1979; Yardley, 1977). The authors are unaware of any examples of staurolite–sillimanite assemblages in which both minerals appear to have grown independently and contemporaneously from matrix minerals, or developed concurrently at a staurolite+sillimanite-in isograd upgrade of lower grade, chlorite-bearing rocks. Equally, no examples are known to the authors of sillimanite-only assemblages, or a sillimanite-in isograd, immediately upgrade of a chlorite-bearing precursor assemblage or metamorphic zone.

Most samples containing staurolite and sillimanite show evidence for consumption of staurolite via domainal subreactions in which staurolite crystals become replaced by muscovite- or plagioclase-rich pseudomorphs and sillimanite grows in separate domains elsewhere in the rock (Carmichael, 1969; Dutrow, Foster, & Whittington, 2008; Foster, 1977, 1981, 1999; Guidotti, 1968; Yardley, 1977). In addition to the numerous examples provided in the above papers, two examples from the Nelson aureole are shown in Figure 4e,f. Growth of garnet accompanying these textures is sometimes indicated by sillimanite inclusions in garnet rims (Figure 4e), consistent with progress of reaction 2.

5 | ISOGRADS MARKING THE INCOMING OF STAUROLITE AND Al_2SiO_5

In a number of Barrovian staurolite–kyanite sequences, the textural evidence for independent, contemporaneous growth of staurolite and kyanite is matched by the mapping of a staurolite+kyanite-in isograd, rather than a distinct kyanite-in isograd upgrade of a staurolite zone as predicted in the phase diagrams in Figure 1. Examples of staurolite+kyanite-in isograds in biotite-bearing rocks (i.e. pelites of normal composition) include the Connecticut Valley Synclinorium of central Vermont (Doll, Cady, Thompson, & Billings, 1961); northern Vermont (Albee, 1968); the Massachusetts–Connecticut border region (Thompson & Norton, 1968); the Esplanade and Mica Creek areas, British Columbia (Digel et al., 1998; Ghent, 1975; Ghent et al., 1977); the eastern Lepontine Alps (Nagel et al., 2002); the Kwoiek area, British Columbia (Hollister, 1969); and the Penfold Creek area, British Columbia (Fletcher & Greenwood, 1979). On the other hand, a staurolite isograd and distinct staurolite zone downgrade of a kyanite isograd/zone occur in many other Barrovian areas, including in the Scottish Barrovian zones (Chinner, 1965; Harte, 1987; McLellan, 1985). Relatively narrow staurolite zones downgrade of the incoming of kyanite are mapped in the Whetstone Lake area, Ontario (Carmichael, 1970) and Dutchess County, New York (Whitney et al., 1996). The mapped location of isograds depends variously on sampling density, distribution on the ground of appropriate bulk compositions and in some cases on mineral assemblages developed in unusual bulk compositions like those described in Section 2.2. Nevertheless, it is clear that there are many settings where staurolite and kyanite first appear in much closer succession than is implied by equilibrium calculation.

In Buchan sequences, staurolite+andalusite-in isograds, rather than sequential staurolite-in and andalusite-in isograds, are also reported. Examples include the Shelburne area, Nova Scotia (Raeside & Jamieson, 1992), the Augusta area, Maine (Osberg, 1968, 1974) and the Nelson aureole (Pattison & Tinkham, 2009). On the other hand, a separate, albeit relatively narrow, staurolite zone downgrade of a staurolite+andalusite zone has been mapped at Harpswell Neck, Maine (Lang & Dunn, 1990) and in other localities described in Pattison and Tracy (1991). From a thermodynamic perspective, coincident or closely spaced staurolite-in and andalusite-in isograds in Buchan settings are less anomalous than coincident or closely spaced staurolite-in and kyanite-in isograds in Barrovian sequences because the thermodynamically predicted separation in temperature between the staurolite-forming reaction (reaction 9) and the Al_2SiO_5-forming reaction (reaction 2) in the andalusite field is less than 20°C (Figure 1c).

As noted above, the authors are unaware of any examples of coincident staurolite+sillimanite-in, or sillimanite-in, isograds upgrade of low-grade chlorite-bearing zones. Rather, sillimanite is observed to develop upgrade of the first appearance of one or some of staurolite, andalusite and kyanite (and at low pressure, cordierite).

6 | WIDTH OF ZONES OF COEXISTING STAUROLITE AND KYANITE OR ANDALUSITE

Many Barrovian sequences have a relatively wide zone of coexistence of staurolite and kyanite, commonly termed a “staurolite+kyanite” zone. Examples include most of the localities described in Section 5 above. This observation differs from the predicted pattern assuming equilibrium (Figure 1c), where a narrow interval of coexistence of staurolite and kyanite (reaction 2) is predicted, separating wider zones of stability of staurolite only (at lower grade) and kyanite only (at higher grade). Complementary to this observation is the general lack of measured compositional variation of minerals going through the transition from a staurolite zone (where it exists), to a kyanite+staurolite zone, to a staurolite-free kyanite zone (where it exists). Compared to the significant predicted changes with grade in Mg/(Mg+Fe) of biotite and staurolite going through Fe–Mg divariant reaction 2, and in related Fe–Mg divariant reactions at lower grade that produce staurolite from chlorite (Thompson, 1976; Tinkham et al., 2001; White, Powell, Holland, et al., 2014), commonly there is little change in the measured compositions (e.g. Craw, 1978; Lang & Rice, 1985).

Within the kyanite zone of the Scottish Barrovian sequence, Chinner (1965) noted that staurolite-free kyanite-bearing assemblages tended to be a little more magnesian, based on the Mg/(Mg+Fe) ratio of biotite, than staurolite+kyanite-bearing from the same zone (0.50–0.56 *v.* 0.52 respectively). On the other hand, these values overlapped with staurolite-bearing assemblages of immediately lower grade (0.54–0.57). McLellan (1985) measured the Mg/(Mg+Fe) ratio of biotite from a larger number of samples from the kyanite zone and found that the mean (*n*; range) of kyanite-only assemblages was 0.55 (13; 0.50–0.63) *v.* 0.48 (26; 0.40–0.66) for staurolite+kyanite assemblages. Yet, the spatial distribution of the two mineral assemblages, and the compositions of their biotite, show little if any pattern with respect to grade (figure 8 of McLellan, 1985). Even if there were a consistent grade-related pattern in composition, the mean difference in terms of Mg/(Mg+Fe) is <0.1, which translates to a rather modest displacement of reaction 2 of <15°C (Figure 1d). The implication is that the broad zone of coexistence of staurolite and kyanite in the Scottish Barrovian sequence, and most likely in other Barrovian sequences, cannot be explained by compositional variation in an equilibrium model. In Buchan sequences, wide zones of coexistence of staurolite and andalusite are also commonly observed, noteworthy examples including the Nelson aureole, Harpswell Neck region, Shelburne area and Augusta area (references above).

7 | PERSISTENCE OF STAUROLITE INTO THE SILLIMANITE ZONE

Staurolite is observed to persist upgrade into the sillimanite zone in Barrovian and Buchan sequences that develop kyanite+staurolite or andalusite+staurolite mineral assemblages downgrade of the first development of sillimanite. According to equilibrium, staurolite should be unstable relative to kyanite or andalusite in such assemblages. In contrast, the demise of staurolite is usually accompanied by a marked increase in sillimanite. Examples include, for kyanite-bearing sequences, the Scottish Barrovian zones (Harte & Johnson, 1969; McLellan, 1985), the Azure Lake area of British Columbia (Pigage, 1982), Dutchess County, New York (Whitney et al., 1996), the Park Ranges, British Columbia (Craw, 1978), Whetstone Lake (Carmichael, 1970), Lepontine Alps (Nagel et al., 2002) and the Kootenay Lake Barrovian sequence, British Columbia (Moynihan & Pattison, 2013; Webster & Pattison, 2018). A counter-example is the Mica Creek area of British Columbia, where the staurolite-out isograd occurs in the kyanite zone. For andalusite-bearing sequences, examples of the persistence of staurolite into the sillimanite zone include the Nelson aureole and Harpswell Neck (references above). Whether in Barrovian or Buchan sequences, the demise of staurolite occurs downgrade of the reaction of muscovite+quartz to Al_2SiO_5+K-feldspar (rare exceptions are discussed in Ashworth, 1975).

8 | SUMMARY OF INCONGRUITIES BETWEEN THERMODYNAMIC PREDICTION AND NATURAL OBSERVATIONS

Summarizing Sections 3–7, the development of staurolite+Al_2SiO_5-bearing mineral assemblages and related zonal sequences differ from predictions from equilibrium phase diagrams in the following ways:

1. Rarity of staurolite-to-sillimanite sequences with neither kyanite nor andalusite anywhere in the sequence, in contrast to the ~2.5 kbar wide interval predicted for such sequences according to equilibrium.
2. Lack of textural evidence of reaction of staurolite to kyanite via the reaction predicted to introduce kyanite to pelites of normal composition (reaction 2 in Figure 1). This observation also pertains to staurolite+andalusite-bearing assemblages, although there are more examples of a reaction relationship between staurolite and andalusite than between staurolite and kyanite.
3. Near-simultaneous incoming of staurolite and kyanite in a number of Barrovian sequences, rather than a broad predicted staurolite zone downgrade of the incoming of kyanite. However, staurolite zones downgrade of the first development of kyanite are also common. Simultaneous incoming of staurolite and andalusite is noted in a number of Buchan sequences.
4. Greater width of zones of coexistence of staurolite and kyanite in Barrovian sequences, and of staurolite and andalusite in Buchan sequences, than predicted, and a lack of consistent mineral-compositional change through these intervals.
5. Persistence of staurolite upgrade until its demise in the sillimanite zone, even in Barrovian and Buchan sequences that develop kyanite+staurolite or andalusite+staurolite mineral assemblages downgrade of the first development of sillimanite.

These incongruities contribute to what has become known as “the staurolite problem” (Pigage & Greenwood, 1982), originally identified based on the mismatch between experimentally constrained staurolite phase equilibria and *P–T* estimates of natural rocks from classical thermobarometry (e.g. Carmichael, 1978; Lang & Rice, 1985; Pigage & Greenwood, 1982). In the next section, we explore possible explanations for the above incongruities.

9 | INTERPRETATION OF INCONGRUITIES BETWEEN THERMODYNAMIC PREDICTION AND NATURAL OBSERVATIONS

9.1 | Experimental and thermodynamic data

A key question is whether the experimental data, on which the thermodynamic data used to calculate the phase diagrams in Figure 1 are based, are reliable when it comes to staurolite+Al_2SiO_5 phase equilibria. Staurolite in muscovite-bearing staurolite- and staurolite+Al_2SiO_5-bearing assemblages is an Fe-rich mineral with Mg/(Mg+Fe) typically in the range 0.15–0.25 (Holdaway, Dutrow, & Shore, 1986), so the thermodynamics of Fe-staurolite is key. An important reaction for thermodynamic data extraction for Fe–staurolite is:

$$\mathrm{Fe-St + Qtz \rightarrow Fe-Grt + Al_2SiO_5 + H_2O.}$$

Several experimental studies have examined this reaction (Dutrow & Holdaway, 1989; Ganguly, 1972; Rao & Johannes, 1979; Richardson, 1968). With the exception of some of the Richardson experiments, the position of this reaction seems largely consistent among the studies (Dutrow & Holdaway, 1989; Holdaway, Mukhopadhyay, & Dutrow, 1995; Holland & Powell, 1998; Pigage & Greenwood, 1982), suggesting that the problem does not lie with the experiments, and therefore with the thermodynamic data for Fe-staurolite. The thermodynamic properties of the Mg-end-member of staurolite in the Holland and Powell (1998, 2011) database are based on several experimental studies listed in those papers, especially Fockenberg (1998), with no obvious problems apparent.

9.2 | Extra components

Possible complications comparing natural staurolite-bearing assemblages with those involved in experimental studies revolve around the non-FMASH “extra” components Zn and Mn (Ashworth, 1975; Guidotti, 1970; Holdaway, Dutrow, & Shore, 1986), H (Holdaway, Dutrow, Borthwick, et al., 1986), Li (Dutrow, Holdaway, & Hinton, 1986) and Fe^{3+} (Dyar et al., 1991). Zn in most muscovite-bearing staurolite- and staurolite+Al_2SiO_5-bearing assemblages is generally low (average Zn/(Zn+Mn+Fe+Mg) ≤ ~0.04) and not widely varying (table 4 of Holdaway et al., 1995; table 1 of Pattison, Spear, & Cheney, 1999). Stabilization of staurolite due to elevated Zn may become important in mineral assemblages in which staurolite occurs in unusually small amounts, has largely reacted out (e.g. Guidotti, 1970; McLellan, 1985) or occurs at unusually high grade (Ashworth, 1975; Grant, 1973). The Mn content of staurolite is about the same as Zn (average Mn/(Zn+Mn+Fe+Mg) of ≤~0.04). Displacement of staurolite-bearing equilibria for the common range of Zn and Mn contents results in a modest stabilizing effect (Pattison et al., 1999). The other components require non-routine analysis methods to determine, resulting in fewer data for comparative analysis, and the effects on the phase equilibria have not been examined other than in a qualitative way (e.g. Holdaway, Dutrow, & Shore, 1986). Overall, these “extra” components are unlikely to be the primary determinants of the distribution and behaviour of staurolite+Al_2SiO_5 assemblages.

9.3 | Metastable production of kyanite and andalusite from chlorite consumption, and the influence of nucleation kinetics

Accepting that staurolite is usually not the primary reactant in the initial (lowest grade) formation of kyanite in Barrovian sequences, or of andalusite in staurolite-bearing

Buchan sequences, kyanite or andalusite must have grown from reaction of other minerals. In high-Al pelites, chloritoid is a possibility, but it does not develop in the more abundant lower-Al pelites of concern to this paper, except possibly at low pressure (e.g. Okuyama-Kusunose, 1994). The other porphyroblast phase that commonly occurs in these assemblages is garnet, but textural evidence of its participation as a reactant (e.g. evidence of dissolution) in staurolite+kyanite/andalusite mineral assemblages is typically minimal (e.g. Harte & Johnson, 1969; Pattison & Tinkham, 2009); commonly, it is co-produced with kyanite or andalusite. In general, rocks in which porphyroblasts were reactants for higher grade mineral assemblages have textures indicating their prior presence, something that is lacking in most staurolite–kyanite/andalusite assemblages. This leaves matrix minerals, in particular muscovite and chlorite, as the most likely reactants (Pattison & Tinkham, 2009; Spear & Pattison, 2017).

Reactions that consume muscovite and chlorite and concomitantly produce porphyroblast phases are listed above in Section 2 and illustrated in Figure 1b (KFMASH) and Figure 1c (MnNCKFMASHT). The reactions include, from lowest to highest pressure ($4'$, $5'$ etc. refer to reactions in KFMASH; 4, 5 etc. refer to reactions in MnNCKFMASHT): cordierite-producing reactions $4'$ and 4; Al_2SiO_5-producing reactions $5'$, 5 and 8; staurolite-producing reactions $6'$, 6 and 9; and garnet-producing reactions $7'$ and 7. Apart from reaction 7, which takes place over a broader multivariant interval than the others, these reactions are similar in slope and position and define a narrow band of significant reaction in which there is a marked modal increase in the product porphyroblast phases and concomitant marked loss of chlorite.

Figure 5a–c shows simplifications of Figure 1b on which the metastable extension of reaction 5, the garnet-free chlorite-to-Al_2SiO_5 reaction in MnNCKFMASHT, is shown as a dashed line. Reaction 5 occurs at most 10°C above the thermodynamically predicted chlorite-to-staurolite reaction (reaction 9). If garnet does not participate in reaction 9 because of sluggish rates of garnet dissolution (e.g. Pattison & Tinkham, 2009; Spear & Pattison, 2017), reaction 6 pertains instead (Figure 5b), and the maximum difference is 15°C. Thus, overstepping of the chlorite-to-staurolite reaction by 15°C or less results in an Al_2SiO_5 mineral becoming a thermodynamically viable alternate product phase from the reaction of muscovite and chlorite, as all of the reactions result in a drop in free energy of the system. In this situation, the kinetics of nucleation may play an important role in determining which phase develops.

As noted above in Section 4.1.1., the crystal structure of staurolite consists of kyanite layers alternating with AlO–OH–2FeO layers. During nucleation and growth of staurolite, the assembly of kyanite layers would result in the formation of templates for the nucleation of the mineral kyanite. There might even be a kinetic advantage in assembling the simpler kyanite structure than the more complex staurolite structure. The result may be a reduction in the critical overstep required for kyanite nucleation compared to staurolite, counterbalancing the small thermodynamic advantage of forming staurolite.

This possibility is illustrated in Figure 5d, which plots reaction affinity *v.* temperature for the staurolite- and kyanite-producing reactions (6 and 5, respectively) along the prograde *P–T* path illustrated in Figure 5b (assumed to be isobaric for simplicity). Reaction affinity is the macroscopic energetic driving force for reaction that is needed to overcome kinetic barriers to nucleation and growth (Pattison et al., 2011; Waters & Lovegrove, 2002). For temperature increase, the rate at which reaction affinity builds with overstepping is a function of the entropy change of the reaction and thus varies significantly among reactions (for pressure variation, the rate at which reaction affinity builds with overstepping is a function of the volume change). Examples are shown in figure 2 of Pattison et al. (2011), from which the slopes of reactions 5 and 6 in Figure 5d are taken. The entropy change is normalized to one oxygen in the product porphyroblast to allow comparison between reactions (Waters & Lovegrove, 2002). The entropy change (and thus the A *v.* T slope) of kyanite-producing reaction 5 modestly exceeds that of staurolite-producing reaction 6 because less H_2O is produced in reaction 6 due to staurolite being a hydrous product phase (Pattison et al., 2011; Spear & Pattison, 2017).

Figure 5d shows that metastable kyanite is never more than ~200 J/mol–O from staurolite in terms of thermodynamic stability (as shown by the two arbitrarily placed vertical dashed lines between the two reactions in Figure 5d). This value is less than the average estimate of 300 J/mol–O of affinity required for the nucleation of a porphyroblast (Pattison et al., 2011, p. 969; Spear & Pattison, 2017). If the energetic threshold for kyanite nucleation is ~200 J/mol–O lower than for staurolite nucleation, it could be as favourable energetically to form as staurolite. With increasing degrees of overstepping of the staurolite-forming reaction, the thermodynamic advantage of forming staurolite compared to kyanite diminishes, owing to the different A *v.* T slopes of reactions 5 and 6 (Figure 5d), which would increasingly favour the development of kyanite (see also figure 7 of Spear & Pattison, 2017). Metastable growth of kyanite from chlorite breakdown, independently and approximately contemporaneously with production of staurolite from chlorite breakdown, would account for the lack of textural evidence of reaction between the two minerals and the near-simultaneous incoming of staurolite and kyanite in a number of Barrovian sequences.

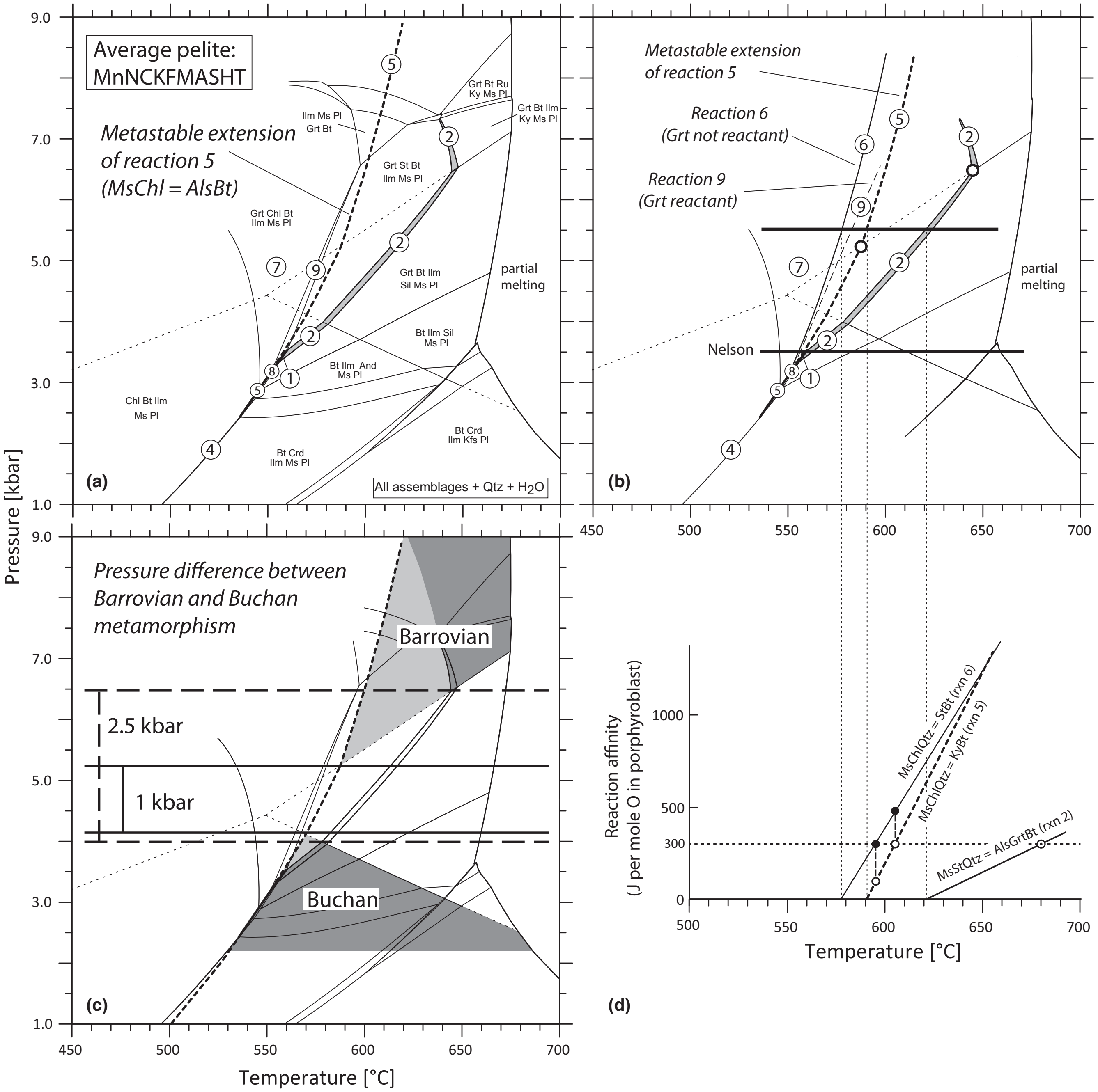

FIGURE 5 (a) Location of metastable extension of reaction 5 (dashed line) superposed on the phase diagram from Figure 1c. (b) Simplified version of (a), showing the position of staurolite-producing reaction 6, in which garnet does not participate, relative to reactions 5 and 9. Bold line at 5.5 kbar is a schematic *P–T* path corresponding to the A *v.* T diagram in (d). The horizontal bold line at 3.5 kbar is the *P–T* path for the Nelson aureole from Pattison and Tinkham (2009). The two open circles are intersections referred to in the text. (c) Diagram illustrating the degree to which the inferred pressure difference between Barrovian (kyanite-bearing) and Buchan (andalusite-bearing) metamorphism decreases from 2.5 to 1 kbar if reaction 5 rather than reaction 2 controls the initial (low-grade) development of Al_2SiO_5 minerals, especially kyanite. The dark-shaded regions are the predicted stability fields for kyanite- and andalusite-bearing assemblages assuming equilibrium (Figure 1c), whereas the light-shaded regions are the predicted stability fields for kyanite- and andalusite-bearing assemblages for kyanite and andalusite growth by reaction 5. (d) Reaction affinity *v.* temperature diagram corresponding to the *P–T* path in (b). Slopes of reactions come from Pattison et al. (2011) (see text for discussion). Intersections of the reactions at zero affinity (= no overstepping) correspond to the positions of the reactions in (b), as shown by the vertical dotted lines joining the two diagrams. The horizontal dashed line at 300 J/mol-O is the average estimate of the energetic threshold for nucleation of a porphyroblast from Pattison et al. (2011). Vertical dashed lines between the open and filled circles on reactions 5 and 6, respectively, represent the difference in affinity between the two reactions at different degrees of overstepping of reaction 6

Concerning staurolite and andalusite, which are predicted to coexist at pressures less than ~4 kbar (Figure 1), the predicted temperature separation between staurolite-producing reaction 6 or 9, and metastable andalusite-producing reaction 5, is <5°C (Figure 5b). The result is an even smaller thermodynamic difference between the two minerals (<~100 J/mol–O) than between kyanite and staurolite, and a smaller degree of overstepping required before andalusite-producing reaction 5 overtakes staurolite-producing reaction 6 in terms of reaction affinity (see figure 18b of Pattison & Tinkham, 2009 and figure 8 of Spear & Pattison, 2017). However, from a kinetic perspective, the difference in the crystallographic structure of andalusite compared to kyanite (and to the kyanite-structured Al_2SiO_5 layers in staurolite) means andalusite would likely be a less favourable alternative to staurolite than kyanite, potentially cancelling out the thermodynamic advantage.

A question concerning the global application of the above hypothesis is why Al_2SiO_5-free, especially kyanite-free, staurolite zones are as prevalent as they are. While not having a simple answer to this question, it seems likely that it depends on the interplay among a number of thermodynamic and kinetic factors that may be particular to each natural situation. Local variations in the composition and nature of grain boundary microdomains may influence which mineral forms a viable nucleus. Kyanite has been shown to be favoured in Mg-richer bulk compositions (Chinner, 1965; McLellan, 1985; Naggar & Atherton, 1970), although the observed compositional difference of these compared to the Fe-richer bulk compositions that develop staurolite-only assemblages is modest (see Section 6 above), usually less than Mg/(Mg+Fe) = 0.1, equivalent to a temperature displacement of <15°C for reactions 2, 5 or 9 (Figure 1d). A compositional argument would also imply consistent compositional differences between the staurolite and staurolite–kyanite zones of individual Barrovian sequences, and between Barrovian sequences where the zones differ.

The relative timing of staurolite and kyanite growth would appear to be crucial, given that both minerals in this scenario require matrix chlorite as a reactant. If staurolite growth precedes kyanite growth, the chlorite needed to make the kyanite may be exhausted before kyanite has a chance to grow. The variable presence and width of staurolite zones may reflect the success, or not, of kyanite to nucleate before staurolite has grown significantly. Fractionation effects may also play a role. For example, fractional growth of staurolite and, where present, garnet, both of which are Fe-rich minerals and which commonly show little evidence for participation as reactants in staurolite–kyanite assemblages, could result in residual chlorite becoming sufficiently magnesian to form kyanite. Pattison and Tinkham (2009, p. 275) proposed such a mechanism to explain andalusite–staurolite–garnet assemblages in which inclusion relationships suggest a time sequence of garnet followed by staurolite followed by andalusite, yet showed no textural evidence of the participation of garnet or staurolite as reactants. Whether staurolite-only or staurolite+kyanite assemblages form might thus be a function of where in this fractionation process chlorite is consumed.

As noted above, increasing degrees of overstepping of the chlorite-consuming, staurolite-forming reaction will favour kyanite or andalusite as an alternative to staurolite. A possible example where this factor may have come into play is the Glacier Creek aureole in British Columbia. Kyanite+staurolite assemblages, in which staurolite shows no evidence for reaction to kyanite, are restricted to the innermost, highest grade part of the aureole, upgrade of a wide staurolite-only domain (D.R.M. Pattison, unpublished data). Figure 3f,g shows photomicrographs of kyanite+staurolite assemblages from the aureole, with Figure 3g illustrating topotaxial intergrowth of kyanite and staurolite suggestive of simultaneous development of the two minerals. It may be that faster heating rates in the inner aureole led to greater degrees of overstepping of the chlorite-to-staurolite reaction, favouring the development of kyanite, whereas further out in the aureole, where heating rates were slower, overstepping was not as great and staurolite alone developed. Such a scenario might be contemplated for regional settings in which advection of heat by magmas is interpreted (i.e. regional contact aureoles), such as proposed for the Scottish Barrovian zones (Baxter et al., 2002; Viete et al., 2013).

9.4 | Kinetic controls on staurolite consumption

The anomalously wide zones of coexistence of staurolite and either kyanite (Barrovian settings) or andalusite (Buchan settings), and the commonly observed demise of staurolite in the sillimanite zone, imply disequilibrium processes as well. However, the controlling kinetic factors differ from those discussed in Section 9.3.

The reaction of staurolite to Al_2SiO_5, typically accompanied by growth of garnet, is ascribed to reaction 2 as noted in Section 4. Figure 5d shows the rate of buildup of reaction affinity with overstepping for reaction 2. Because reaction 2 only releases a little water, it has a low entropy change and thus a relatively shallow slope in Figure 5d (Pattison et al., 2011). Reaction 2 therefore builds up reaction affinity more slowly than reactions 5 and 6, from which it can be inferred that the amount of overstepping in temperature needed to effect significant reaction by reaction 2 is likely to be greater than for reactions 5 and 6. For example, for an arbitrary energetic barrier to nucleation of 300 J/mol–O (horizontal dashed line in Figure 5d), reaction 5 or 6 requires ~20°C of overstepping to build affinity to this level, whereas reaction 2 requires ~60°C of overstepping. The low rate of buildup of reaction affinity may therefore partially account for the observed delayed reaction of staurolite to Al_2SiO_5 (cf. figure 18b of Pattison & Tinkham, 2009; figure 8d of Spear & Pattison, 2017).

Another factor relates to the behaviour of kyanite or andalusite if they grow metastably from chlorite consumption (reaction 5) in the staurolite stability field, as argued in Section 9.3. In this situation, kyanite or andalusite will be metastable relative to staurolite, and therefore predicted thermodynamically to react to staurolite, rather than vice versa, until temperature rises and conditions of reaction 2 have been achieved. A significant difference between Barrovian staurolite+kyanite sequences and Buchan staurolite+andalusite sequences is the width of the predicted staurolite stability field where this process may occur (between the incoming of staurolite by chlorite-consuming reactions 6 or 9, and the onset of the staurolite-to-Al_2SiO_5 reaction, reaction 2). The width of the staurolite zones reaches a maximum (~60°C) where reaction 2 intersects the kyanite–sillimanite boundary (Figure 5), whereas in the andalusite field, it is ~20°C or less.

For the representative Barrovian *P–T* path shown in Figure 5b, the temperature difference between metastable kyanite-producing reaction 5 and staurolite-consuming reaction 2 is ~30°C. If kyanite forms metastably from reaction 5 because of favourable nucleation kinetics, the tendency according to thermodynamics will be for the metastable kyanite to react to form stable staurolite by the reverse of reaction 2 (or its garnet-free equivalent). The free energy driving force for this process will be at its greatest where kyanite develops in the low-*T* part of the staurolite zone, diminishing as temperature rises and reaction 2 (and Al_2SiO_5 stability) is approached. In the authors' experience, there is little evidence for "back reaction" of kyanite to staurolite, although one of the reviewers of this paper (C.T. Foster) suggested that the texture in Figure 3h, in which euhedral staurolite is intergrown with anhedral kyanite, could be interpreted as staurolite replacing kyanite. Lack of reaction of kyanite to staurolite is anticipated for several reasons: the relatively small free energy change of reaction 2, as noted above; the likely absence of significant free H_2O, a necessary reactant to form hydrous staurolite, in the pore space of the rock; and the kinetic difficulty of dissolving kyanite and, if it is present and participates, garnet. The expected result is a broad staurolite+kyanite zone showing little textural or compositional evidence for reaction, as commonly observed.

In such sequences, staurolite typically shows little evidence for reaction until its demise in the sillimanite zone. If kyanite develops at relatively low grade from chlorite breakdown, this observation is consistent with *P–T* passage anywhere through the ~5.0–6.5 kbar pressure interval between (1) the intersection of reaction 5 and the kyanite–sillimanite boundary and (2) the intersection of reaction 2 with the kyanite–sillimanite boundary (unfilled circles in Figure 5b), such as along the *P–T* path in Figure 5b. For such *P–T* paths, staurolite is predicted to break down to sillimanite by reaction 2, as observed. The kyanite–sillimanite reaction is also crossed by such paths, but the sluggish kinetics of the polymorphic inversion reaction may result in no significant reaction progress. For a *P–T* path at higher pressure, where reaction 2 occurs in the kyanite stability field, such as at Mica Creek, British Columbia, staurolite is predicted to react to kyanite rather than sillimanite, although no textural evidence for progress of this reaction has been reported there.

In the case of andalusite-bearing Buchan sequences, reaction 2 is <15°C higher than reaction 5 (Figure 5b), meaning that if andalusite forms metastably by reaction 5, only a little further temperature rise is needed to reach conditions of reaction 2, at which point staurolite is predicted to react to andalusite. In the Nelson aureole, a wide zone of coexisting staurolite and andalusite extends well upgrade of the thermodynamically predicted onset of reaction 2 (figure 14 of Pattison & Tinkham, 2009). The *P–T* path at Nelson is shown on Figure 5b as a solid horizontal line. The staurolite+andalusite zone terminates immediately upgrade of the sillimanite-in isograd, above which there is a volumetric reduction in staurolite and increase in sillimanite, accompanied by garnet growth, in a relatively narrow interval (figures 1 and 15 of Pattison & Tinkham, 2009). Downgrade of the sillimanite isograd, within the staurolite+andalusite zone, localized, patchy reaction of staurolite to andalusite occurs at a range of scales, including individual thin sections where one part of a thin section may contain euhedral, unreacted staurolite porphyroblasts and millimetres away otherwise identical staurolite porphyroblasts show partial to complete pseudomorphism by andalusite (figure 3c–e of Pattison & Tinkham, 2009). In the absence of compositional variations, these authors attributed this observation to localized catalysis of the staurolite-to-andalusite reaction, most likely by fluid. The patchy reaction of staurolite to andalusite demonstrates that staurolite was indeed metastable relative to andalusite in the staurolite+andalusite zone, yet did not react volumetrically to andalusite, an observation ascribed to some or all of slow rate of buildup of reaction affinity of reaction 2; sluggish dissolution of staurolite; difficulty of nucleation of andalusite; and lack of fluid presence to catalyse reaction, except locally (Pattison & Tinkham, 2009, p. 276).

The relatively abrupt demise of staurolite immediately upgrade of the sillimanite isograd at Nelson and in other in Buchan settings suggests an acceleration in the rate of reaction 2 related to different nucleation kinetics of sillimanite and andalusite. Sillimanite in most metamorphic rocks is finer grained and more widely distributed compared with discrete porphyroblasts of andalusite. Both of these factors would favour progress of staurolite consumption by reaction 2: large numbers of small sillimanite crystals would provide more available growth surfaces than discrete andalusite porphyroblasts, and smaller transport distances from the dissolving reactant phase (staurolite) to the product phase (sillimanite) would facilitate intergranular mass transfer between staurolite and sillimanite. Such an explanation could also pertain to high-pressure Barrovian sequences that traverse reaction 2 in the kyanite stability field, yet may not show evidence for reaction of staurolite until sillimanite becomes stable. The onset of volumetric demise of staurolite may therefore be controlled by when sillimanite develops, or becomes stable.

9.5 | Summary

In Sections 9.3 and 9.4, we argue that disequilibrium processes provide the best explanation for the mismatch between the predictions from equilibrium phase diagrams and the observed features of staurolite+Al_2SiO_5-bearing assemblages and zonal sequences. The essential elements are the appearance of staurolite and Al_2SiO_5 minerals (particularly kyanite) in much closer succession, and with much wider coexistence, than is implied by equilibrium calculation, augmented by textural incongruities and a mismatch between predicted and observed occurrences of staurolite–sillimanite sequences with neither kyanite nor andalusite developed anywhere in the sequence. Several of these mismatches can be accounted for by metastable growth of kyanite or andalusite from chlorite consumption after small degrees of overstepping (as little as 10–15°C) of the stable chlorite-to-staurolite reaction, augmented, in the case of kyanite, by especially favourable nucleation kinetics. The unusual width of coexistence of staurolite and Al_2SiO_5 minerals, in particular kyanite and andalusite, can be accounted for by a combination of lack of sufficient thermodynamic driving force for conversion of staurolite to kyanite or andalusite, sluggish dissolution of staurolite and possibly the absence of a fluid phase to catalyse reaction.

10 | IMPLICATIONS

If the foregoing is accepted, there are a number of implications:

1. Disequilibrium processes need to be considered in regional metamorphism as well as contact metamorphism. Although we do not question that equilibrium thermodynamics is the primary control on the development of "peak" metamorphic mineral assemblages—a fact demanded by the metamorphic facies principle—it seems that the "continuous equilibrium" model of prograde metamorphism, in which metamorphic mineral assemblages are never far from their predicted equilibrium state throughout their prograde history, is more open to question. Viewing the development of metamorphic mineral assemblages as an interplay between equilibrium and kinetics will probably result in the best interpretations.
2. Barrovian kyanite–staurolite assemblages, and by extension Barrovian metamorphic sequences, may form at lower pressure and temperature than currently implied in equilibrium phase diagrams calculated with commonly used thermodynamic databases and *a–x* relations. This point is illustrated in Figure 5c: instead of minimum *P–T* conditions of ~630°C, ~6.5 kbar for staurolite–kyanite assemblages, they may develop as low as ~580°C, ~5 kbar if developed from chlorite-consuming reactions, assuming the current thermodynamic data and *a–x* relations are accurate. A consequence is that kyanite-bearing Barrovian mineral assemblage zones and andalusite-bearing Buchan-type mineral assemblage zones could differ in pressure by as little as ~1 kbar, rather than by ~2.5 kbar as currently predicted. The rarity of staurolite–sillimanite sequences with neither kyanite nor andalusite developed anywhere in the sequence suggests that the pressure difference could be even less. Estimates of the pressure–temperature conditions of Barrovian staurolite+kyanite mineral assemblages that assume they developed only by reactions predicted in equilibrium phase diagrams may need to be reconsidered.

ACKNOWLEDGEMENTS

We acknowledge Journal reviewers D. Waters and T. Foster for their insightful reviews that significantly improved the presentation and content of the paper. Waters's comments on nucleation kinetics were especially influential. We thank B. Harte and D. Carmichael for their unofficial, detailed reviews that sharpened our arguments. By acknowledging these individuals, we do not imply that they agree with everything we have written. M. Brown provided typically helpful editorial oversight. This research was supported by NSERC Discovery Grant 037233 to Pattison and NSF grant 1447468 to Spear.

CONFLICT OF INTEREST

The authors have no conflict of interest to declare.

ORCID

David R. M. Pattison http://orcid.org/0000-0001-5817-6373
Frank S. Spear http://orcid.org/0000-0002-5745-4957

REFERENCES

Ague, J. J. (1991). Evidence for major mass transfer and volume strain during regional metamorphism of pelites. *Geology*, *19*, 855–858. https://doi.org/10.1130/0091-7613(1991)019<0855:EFMMTA>2.3.CO;2

Ague, J. J., & Baxter, E. F. (2007). Brief thermal pulses during mountain building recorded by Sr diffusion in apatite and multicomponent diffusion in garnet. *Earth and Planetary Science Letters*, *261*, 500–516. https://doi.org/10.1016/j.epsl.2007.07.017

Albee, A. L. (1968). Metamorphic zones in northern Vermont. In E-an Zen, W. S. White, J. B. Hadley, & J. B. Thompson (Eds.), *Studies of Appalachian geology – Northern and maritime* (pp. 329–342). New York, NY: John Wiley and Sons.

Ashworth, J. R. (1975). Staurolite at anomously high grade. *Contributions to Mineralogy and Petrology*, *53*, 281–291. https://doi.org/10.1007/BF00382444

Bailes, A. H., & McRitchie, W. D. (1978). The transition from low to high grade metamorphism in the Kisseynew sedimentary gneiss belt, Manitoba. In J. A. Fraser & W. W. Heywood (Eds.), *Metamorphism in the Canadian shield. Geological Survey of Canada Paper*, *78-10*, 155–179.

Baxter, E. F., Ague, J. J., & DePaolo, D. J. (2002). Prograde temperature–time evolution in the Barrovian type-locality constrained by Sm/Nd garnet ages from Glen Clova, Scotland. *Journal of the Geological Society*, *159*, 71–82. https://doi.org/10.1144/0016-76901013

Beiter, T., Wagner, T., & Markl, G. (2008). Formation of kyanite-quartz veins of the Alpe Sponda, Central Alps, Switzerland: Implications for Al transport during regional metamorphism. *Contributions to Mineralogy and Petrology*, *156*, 689–707. https://doi.org/10.1007/s00410-008-0310-4

Berman, R. G. (1988). Internally-consistent thermodynamic data for minerals in the system $Na_2O–K_2O–CaO–MgO–FeO–Fe_2O_3–Al_2O_3–SiO_2–TiO_2–H_2O–CO_2$. *Journal of Petrology*, *29*, 445–522. https://doi.org/10.1093/petrology/29.2.445

Briggs, W., & Foster, C. T. (1992). Pressure-temperature conditions of Early Proterozoic metamorphism during the Trans-Hudson Orogen as determined from rocks straddling the Flin Flon – Kisseynew boundary at Niblock and File lakes, Manitoba. *Canadian Journal of Earth Sciences*, *29*, 2497–2507. https://doi.org/10.1139/e92-196

Carlson, W. D., Pattison, D. R. M., & Caddick, M. J. (2015). Beyond the equilibrium paradigm: How consideration of kinetics enhances metamorphic interpretation. *American Mineralogist*, *100*, 1659–1667. https://doi.org/10.2138/am-2015-5097

Carmichael, D. M. (1969). On the mechanism of prograde metamorphic reactions in quartz-bearing pelitic rocks. *Contributions to Mineralogy and Petrology*, *20*, 244–267. https://doi.org/10.1007/BF00377479

Carmichael, D. M. (1970). Intersecting isograds in the Whetstone Lake area, Ontario. *Journal of Petrology*, *11*, 147–181. https://doi.org/10.1093/petrology/11.1.147

Carmichael, D. M. (1978). Metamorphic bathozones and bathograds: A measure of the depth of post metamorphic uplift and erosion on the regional scale. *American Journal of Science*, *278*, 769–797. https://doi.org/10.2475/ajs.278.6.769

Chinner, G. A. (1961). The origin of sillimanite in Glen Clova, Angus. *Journal of Petrology*, *2*, 312–323. https://doi.org/10.1093/petrology/2.3.312

Chinner, G. A. (1965). The kyanite isograd in Glen Clova, Angus, Scotland. *Mineralogical Magazine*, *34*, 132–143. https://doi.org/10.1180/minmag.1965.034.268.11

Coggon, R., & Holland, T. J. B. (2002). Mixing properties of phengitic micas and revised garnet–phengite thermobarometers. *Journal of Metamorphic Geology*, *20*, 683–696. https://doi.org/10.1046/j.1525-1314.2002.00395.x

Connolly, J. A. D., & Cesare, B. (1993). C-O–H–S fluid compositions and oxygen fugacity in graphitic metapelites. *Journal of Metamorphic Geology*, *11*, 379–388. https://doi.org/10.1111/j.1525-1314.1993.tb00155.x

Craw, D. (1978). Metamorphism, structure and stratigraphy in the southern Park ranges, British Columbia. *Canadian Journal of Earth Sciences*, *15*, 86–98. https://doi.org/10.1139/e78-008

de Capitani, C., & Brown, T. H. (1987). The computation of chemical equilibria in complex systems containing non-ideal solutions. *Geochimica et Cosmochimica Acta*, *51*, 2639–2652. https://doi.org/10.1016/0016-7037(87)90145-1

de Capitani, C., & Petrakakis, K. (2010). The computation of equilibrium assemblage diagrams with Theriak/Domino software. *American Mineralogist*, *95*, 1006–1016. https://doi.org/10.2138/am.2010.3354

Digel, S. G., Ghent, E. D., Carr, S. D., & Simony, P. S. (1998). Early Cretaceous kyanite-sillimanite metamorphism and Paleocene sillimanite overprint near Mount Cheadle, southeastern British Columbia: Geometry, geochronology, and metamorphic implications. *Canadian Journal of Earth Sciences*, *35*, 1070–1087. https://doi.org/10.1139/e98-052

Doll, C. G., Cady, W. M., Thompson, J. B., & Billings, M. P. (1961). *Centennial geologic map of Vermont*. Montpelier, VT: Vermont Geological Survey.

Dutrow, B. L., Foster, C. T., & Whittington, J. (2008). Prograde muscovite-rich pseudomorphs as indicators of conditions during metamorphism: An example from NW Maine. *American Mineralogist*, *93*, 300–314. https://doi.org/10.2138/am.2008.2621

Dutrow, B. L., & Holdaway, M. L. (1989). Experimental determination of the upper thermal stability of Fe-staurolite + quartz at medium pressures. *Journal of Petrology*, *30*, 229–248. https://doi.org/10.1093/petrology/30.1.229

Dutrow, B. L., Holdaway, M. J., & Hinton, R. W. (1986). Lithium in staurolite and its petrologic significance. *Contributions to Mineralogy and Petrology*, *94*, 496–506. https://doi.org/10.1007/BF00376341

Dyar, M. D., Perry, C. L., Rebbert, C. R., Dutrow, B. L., Holdaway, M. J., & Lang, H. M. (1991). Mössbauer spectroscopy of synthetic and naturally occurring staurolite. *American Mineralogist*, *76*, 27–41.

Farber, K. (2011). Mechanism of mineral reactions and element mobility during Barrovian metamorphism. Unpublished MSc thesis, Westfälische Wilhelms-Universität Münster.

Farber, K., Caddick, M. J., & John, T. (2014). Controls on solid-phase inclusion during porphyroblast growth: Insights from the

Barrovian sequence (Scottish Dalradian). *Contributions to Mineralogy and Petrology*, *168*, 17

Ferraris, G., Makovicky, E., & Merlino, S. (2004). Crystallography of modular materials. (p. 266). Oxford: Oxford University Press.

Fletcher, C. J. N., & Greenwood, H. J. (1979). Metamorphism and structure of Penfold Creek area, near Quesnel Lake, British Columbia. *Journal of Petrology*, *20*, 743–794. https://doi.org/10.1093/petrology/20.4.743

Flinn, D., Key, R. M., & Khoo, T. T. (1996). The chloritoid schists of Shetland and their thermal metamorphism. *Scottish Journal of Geology*, *32*, 67–82. https://doi.org/10.1144/sjg32010067

Fockenberg, T. (1998). An experimental investigation on the P-T stability of Mg-staurolite in the system MgO–Al_2O_3–SiO_2–H_2O. *Contributions to Mineralogy and Petrology*, *130*, 187–198. https://doi.org/10.1007/s004100050359

Foster, C. T. (1977). Mass transfer in sillimanite-bearing pelitic schists near Rangeley, Maine. *American Mineralogist*, *62*, 727–746.

Foster, C. T. (1981). A thermodynamic model of mineral segregations in the lower sillimanite zone near Rangeley, Maine. *American Mineralogist*, *66*, 260–277.

Foster, C. T. (1999). Forward modeling of metamorphic textures. *Canadian Mineralogist*, *37*, 415–429.

Fox, J. S. (1975). Three dimensional isograds from the Lukmanier Pass, Switzerland, and their tectonic significance. *Geological Magazine*, *112*, 547–626. https://doi.org/10.1017/S0016756800038966

Froese, E., & Gasparrini, E. (1975). Metamorphic zones in the Snow Lake area, Manitoba. *Canadian Mineralogist*, *13*, 162–167.

Froese, E., & Moore, J. M. (1980). Metamorphism in the Snow Lake area, Manitoba. Geological Survey of Canada Paper, *78-27*, 21.

Gaidies, F., Pattison, D. R. M., & de Capitani, C. (2011). Towards a quantitative model of metamorphic nucleation and growth. *Contributions to Mineralogy and Petrology*, *162*, 975–993. https://doi.org/10.1007/s00410-011-0635-2

Ganguly, J. (1972). Staurolite stability and related parageneses: Theory, experiments, and applications. *Journal of Petrology*, *13*, 335–365. https://doi.org/10.1093/petrology/13.2.335

Ghent, E. D. (1975). Temperature, pressure and mixed volatile equilibria attending metamorphism of staurolite-kyanite-bearing assemblages, Esplanade Range, British Columbia. *Geological Society of America Bulletin*, *86*, 1654–1660. https://doi.org/10.1130/0016-7606(1975)86<1654:TPAMEA>2.0.CO;2

Ghent, E. D., Simony, P. S., Mitchell, W., Perry, J., Robbins, D., & Wagner, J. (1977). Structure and metamorphism in southeast Canoe River area, British Columbia. *Report of activities, part C. Geological Survey of Canada Paper*, *77-1C*, 13–18.

Gordon, T. M. (1989). Thermal evolution of the Kisseynew sedimentary gneiss belt, Manitoba: Metamorphism at an Early Proterozoic accretionary margin. In J. S. Daly, R. A. Cliff & B. W. D. Yardley (Eds.), *Evolution of metamorphic belts*. *Geological Society of London Special Publication*, *43*, 233–243.

Gordon, T. M., Ghent, E. D., & Stout, M. Z. (1991). Algebraic analysis of the biotite-sillimanite isograd in the File Lake area, Manitoba. *Canadian Mineralogist*, *29*, 673–686.

Grant, J. A. (1973). Phase equilibria in high-grade metamorphism and partial melting of pelitic rocks. *American Journal of Science*, *273*, 289–317. https://doi.org/10.2475/ajs.273.4.289

Guidotti, C. V. (1968). Prograde muscovite pseudomorphs after staurolite in the Rangeley-Oquossoc areas, Maine. *American Mineralogist*, *53*, 1368–1376.

Guidotti, C. V. (1970). The mineralogy and petrology of the transition from the lower to upper sillimanite zone in the Oquossoc area, Maine. *Journal of Petrology*, *11*, 277–336. https://doi.org/10.1093/petrology/11.2.277

Guidotti, C. V. (1974). Transition from staurolite to sillimanite zone, Rangeley Quadrangle, Maine. *Geological Society of America Bulletin*, *85*, 475–490. https://doi.org/10.1130/0016-7606(1974)85<475:TFSTSZ>2.0.CO;2

Guidotti, C. V., & Holdaway, M. J. (1993). Petrology and field relations of successive metamorphic events in pelites of West-central Maine. In J. T. Cheney & J. C. Hepburn (Eds.), *Field trip guidebook for the Northeastern United States*. *Geological Society of America (Boston)*, *1*, L1–L26.

Guidotti, C. V., & Johnson, S. E. (2002). Pseudomorphs and associated microstructures of Western Maine, USA. *Journal of Structural Geology*, *24*, 1139–1156. https://doi.org/10.1016/S0191-8141(01)00097-9

Guidotti, C. V., Teichmann, F., & Henry, D. J. (1991). Chlorite-bearing polymetamorphic metapelites in the Rangely area, Maine. *American Mineralogist*, *76*, 867–879.

Harte, B. (1975). Displacement of the kyanite 'isograd' by local variations of oxygen fugacity within pelitic schists in Glen Lethnot, Angus Scotland. EOS, Program and Abstracts of the Spring Meeting of the American Geophysical Union, V60.

Harte, B. (1987). Excursion 17. Glen Esk Dalradian, Barrovian metamorphic zones. In: H. H. Trewin, B. C. Kneller & C. Gillen, (Eds.), *Excursion guide to the geology of the Aberdeen area*. (pp. 193–210). Edinburgh: Geological Society of Aberdeen - Scottish Academic Press.

Harte, B., Booth, J. E., & Fettes, D. J. (1987). Excursion 18. Stonehaven to Findon: Dalradian structure and metamorphism. In H. H. Trewin, B. C. Kneller & C. Gillen (Eds.), *Excursion guide to the geology of the Aberdeen area*. (pp. 211–226). Edinburgh: Geological Society of Aberdeen - Scottish Academic Press.

Harte, B., & Hudson, N. F. C. (1979). Pelite facies series and the temperatures and pressures of Dalradian metamorphism in E Scotland. In A. L. Harris, C. H. Holland & B. E. Leake (Eds.), *The Caledonides of the British Isles – Reviewed*. *Geological Society of London Special Publication*, *8*, 323–336.

Harte, B., & Johnson, M. R. W. (1969). Metamorphic history of Dalradian rocks in Glens Clova, Esk and Lethonot, Angus, Scotland. *Scottish Journal of Geology*, *5*, 54–80. https://doi.org/10.1144/sjg05010054

Holdaway, M. J. (1978). Significance of chloritoid-bearing and staurolite-bearing rocks in the Picuris Range, New Mexico. *Geological Society of America Bulletin*, *89*, 1404–1414. https://doi.org/10.1130/0016-7606(1978)89<1404:SOCASR>2.0.CO;2

Holdaway, M. J., & Dutrow, B. L. (1989). Significance of Al silicate in staurolite grade rocks, central Maine. New England Intercollegiate Geological Conference, 81st Annual Meeting, 122–143.

Holdaway, M. J., Dutrow, B. L., Borthwick, J., Shore, P., Harmon, R. S., & Hinton, R. W. (1986). H content of staurolite as determined by H extraction line and ion microprobe. *American Mineralogist*, *71*, 1135–1141.

Holdaway, M. J., Dutrow, B. L., & Hinton, R. W. (1988). Devonian and Carboniferous metamorphism in west-central Maine: The muscovite-almandine geobarometer and the staurolite problem revisited. *American Mineralogist*, *73*, 20–47.

Holdaway, M. J., Dutrow, B. L., & Shore, P. (1986). A model for the crystal chemistry of staurolite. *American Mineralogist*, *71*, 1142–1159.

Holdaway, M. J., Mukhopadhyay, B., & Dutrow, B. L. (1995). Thermodynamic properties of stoichiometric staurolite $H_2Fe_4Al_{18}Si_8O_{48}$ and $H_6Fe_2Al_{18}Si_8O_{48}$. *American Mineralogist*, *80*, 520–533. https://doi.org/10.2138/am-1995-5-612

Holland, T. J. B., & Powell, R. (1985). An internally consistent thermodynamic data set with uncertainties and correlations: 2. Data and results. *Journal of Metamorphic Geology*, *3*, 343–370. https://doi.org/10.1111/j.1525-1314.1985.tb00325.x

Holland, T. J. B., & Powell, R. (1990). An enlarged and updated internally consistent thermodynamic dataset with uncertainties and correlations: The system K_2O-Na_2O-CaO-MgO-MnO-FeO-Fe_2O_3-Al_2O_3-TiO_2-SiO_2-C-H_2-O_2. *Journal of Metamorphic Geology*, *8*, 89–124. https://doi.org/10.1111/j.1525-1314.1990.tb00458.x

Holland, T. J. B., & Powell, R. (1998). An internally consistent thermodynamic data set for phases of petrological interest. *Journal of Metamorphic Geology*, *16*, 309–344.

Holland, T. J. B., & Powell, R. (2003). Activity–composition relations for phases in petrological calculations: An asymmetric multicomponent formulation. *Contributions to Mineralogy and Petrology*, *145*, 492–501. https://doi.org/10.1007/s00410-003-0464-z

Holland, T. J. B., & Powell, R. (2011). An improved and extended internally consistent thermodynamic dataset for phases of petrological interest, involving a new equation of state for solids. *Journal of Metamorphic Geology*, *29*, 333–383. https://doi.org/10.1111/j.1525-1314.2010.00923.x

Hollister, L. S. (1969). Contact metamorphism in the Kwoiek Area of B.C.: An end member of the metamorphic process. *Geological Society of America Bulletin*, *80*, 2465–2494. https://doi.org/10.1130/0016-7606(1969)80[2465:CMITKA]2.0.CO;2

Horkley, L. K. S., Spear, F. S., Ruscitto, D., & Tailby, N. (2013). The secret life of kyanite. *Program with abstracts*. Northeast Section of the Geological Society of America

Kerrick, D. M. (1987). Fibrolite in contact aureoles of Donegal, Ireland. *American Mineralogist*, *72*, 240–254.

Kretz, R. (1983). Symbols for rock-forming minerals. *American Mineralogist*, *68*, 277–279.

Lang, H. M., & Dunn, G. R. (1990). Sequential porphyroblast growth during deformation in a low-pressure metamorphic terrain, Orrs Island-Harpswell Neck, Maine. *Journal of Metamorphic Geology*, *8*, 199–216. https://doi.org/10.1111/j.1525-1314.1990.tb00466.x

Lang, H. M., & Rice, J. M. (1985). Geothermometry, geobarometry and T-X(Fe-Mg) relations in metapelites, Snow Peak, Northern Idaho. *Journal of Petrology*, *26*, 889–924. https://doi.org/10.1093/petrology/26.4.889

McLean, D. (1965). The science of metamorphism in metals. In W. S. Pitcher & G. W. Flinn (Eds.), *Controls of metamorphism*. *Geological Journal Special Issue*, *1*, 103–118. Edinburgh: Oliver & Boyd.

McLellan, E. L. (1985). Metamorphic reactions in the kyanite and sillimanite zones of the Barrovian type area. *Journal of Petrology*, *26*, 798–818.

Moynihan, D. P., & Pattison, D. R. M. (2013). Barrovian metamorphism in the central Kootenay Arc, British Columbia: Petrology and isograd geometry. *Canadian Journal of Earth Sciences*, *50*, 769–794. https://doi.org/10.1139/cjes-2012-0083

Nagel, T., de Capitani, C., & Frey, M. (2002). Isograds and P-T evolution in the eastern Lepontine Alps (Graubunden, Switzerland). *Journal of Metamorphic Geology*, *20*, 309–324. https://doi.org/10.1046/j.1525-1314.2002.00368.x

Naggar, M. H., & Atherton, M. P. (1970). The composition and metamorphic history of some aluminium silicate-bearing rocks from the aureoles of the Donegal Granites. *Journal of Petrology*, *11*, 549–589. https://doi.org/10.1093/petrology/11.3.549

Okuyama-Kusunose, Y. (1994). Phase relations in andalusite-sillimanite Fe-rich metapelites: Tono contact metamorphic aureole, northeast Japan. *Journal of Metamorphic Geology*, *12*, 153–168. https://doi.org/10.1111/j.1525-1314.1994.tb00011.x

Osberg, P. H. (1968). Stratigraphy, structural geology, and metamorphism of the Waterville-Vassalboro area, Maine. *Maine Geological Survey Bulletin*, *20*, 64.

Osberg, P. H. (1974). Buchan-type metamorphism of the Waterville pelite, south-central Maine. In P. H. Osberg (Ed.), *Geology of east-central and north-central Maine* (pp. 210–222). Orono, Maine: University of Maine.

Palin, R. M., Weller, O. M., Waters, D. J., & Dyck, B. (2016). Quantifying geological uncertainty in metamorphic phase equilibria modelling: A Monte Carlo assessment and implications for tectonic interpretations. *Geoscience Frontiers*, *7*, 591–607. https://doi.org/10.1016/j.gsf.2015.08.005

Pattison, D. R. M. (1992). Stability of andalusite and sillimanite and the Al_2SiO_5 triple point: Constraints from the Ballachulish aureole, Scotland. *Journal of Geology*, *100*, 423–446. https://doi.org/10.1086/629596

Pattison, D. R. M., de Capitani, C., & Gaidies, F. (2011). Petrologic consequences of variations in metamorphic reaction affinity. *Journal of Metamorphic Geology*, *29*, 953–977. https://doi.org/10.1111/j.1525-1314.2011.00950.x

Pattison, D. R. M., & DeBuhr, C. L. (2015). Petrology of metapelites in the Bugaboo aureole, British Columbia, Canada. *Journal of Metamorphic Geology*, *33*, 437–462. https://doi.org/10.1111/jmg.12128

Pattison, D. R. M., Spear, F. S., & Cheney, J. Y. (1999). Polymetamorphic origin of muscovite + cordierite + staurolite + biotite assemblages: Implications for the metapelitic petrogenetic grid and for P-T paths. *Journal of Metamorphic Geology*, *17*, 685–703. https://doi.org/10.1046/j.1525-1314.1999.00225.x

Pattison, D. R. M., Spear, F. S., DeBuhr, C. L., Cheney, J. T., & Guidotti, C. V. (2002). Thermodynamic modelling of the reaction muscovite + cordierite = Al_2SiO_5 + biotite + quartz + H_2O: Constraints from natural assemblages and implications for the metapelitic petrogenetic grid. *Journal of Metamorphic Geology*, *20*, 99–118. https://doi.org/10.1046/j.0263-4929.2001.356.356.x

Pattison, D. R. M., & Tinkham, D. T. (2009). Interplay between equilibrium and kinetics in prograde metamorphism of pelites: An example from the Nelson aureole, British Columbia. *Journal of Metamorphic Geology*, *27*, 249–279. https://doi.org/10.1111/j.1525-1314.2009.00816.x

Pattison, D. R. M., & Tracy, R. J. (1991). Phase equilibria and thermobarometry of metapelites. In D. M. Kerrick (ed.) *Contact metamorphism. Mineralogical Society of America Reviews in Mineralogy*, *26*, 105-206. https://doi.org/10.1007/978-3-642-76145-4

Pattison, D. R. M., & Vogl, J. J. (2005). Contrasting sequences of metapelitic mineral-assemblages in the aureole of the tilted Nelson Batholith, British Columbia: Implications for phase equilibria and pressure determination in andalusite–sillimanite type settings. *Canadian Mineralogist*, *43*, 51–88. https://doi.org/10.2113/gscanmin.43.1.51

Pigage, L. C. (1982). Linear regression analysis of sillimanite-forming reactions at Azure Lake, British Columbia. *Canadian Mineralogist*, *20*, 349–378.

Pigage, L. C., & Greenwood, H. J. (1982). Internally consistent estimates of pressure and temperature: The staurolite problem. *American Journal of Science*, *282*, 943–969. https://doi.org/10.2475/ajs.282.7.943

Powell, R., Holland, T. J. B., & Worley, B. (1998). Calculating phase diagrams involving solid solutions via non-linear equations, with examples using THERMOCALC. *Journal of Metamorphic Geology*, *16*, 577–588. https://doi.org/10.1111/j.1525-1314.1998.00157.x

Raeside, R. P., & Jamieson, R. A. (1992). Low pressure metamorphism of the Meguma Terrane, Nova Scotia. Geological Association of Canada – Mineralogical Association of Canada Joint Annual Meeting, Wolfville '92, Field Excursion C-5 Guidebook, 25 pp.

Rao, B. B., & Johannes, W. (1979). Further data on the stability of staurolite + quartz and related assemblages. *Neues Jahrbuch fur Mineralogie Monatshefte*, *1979*, 437–447.

Reche, J., Martinez, F. J., Arboleya, M. L., Dietsch, C., & Briggs, W. D. (1998). Evolution of a kyanite-bearing belt within a HT-LP orogen: The case of NW Variscan Iberia. *Journal of Metamorphic Geology*, *16*, 379–394.

Richardson, S. W. (1968). Staurolite stability in a part of the system Fe-Al-Si-O-OH. *Journal of Petrology*, *9*, 467–488. https://doi.org/10.1093/petrology/9.3.467

Ridley, J., & Thompson, A. B. (1986). The role of mineral kinetics in the development of metamorphic microtextures. In J. V. Walther & B. J. Wood (Eds.), *Fluid-rock interactions during metamorphism. Advances in Physical Geochemistry*, *5*, 154–193. New York, NY: Springer-Verlag.

Rubie, D. C. (1986). The catalysis of mineral reactions by water and restrictions on the presence of aqueous fluid during metamorphism. *Mineralogical Magazine*, *50*, 399–415. https://doi.org/10.1180/minmag.1986.050.357.05

Rubie, D. C. (1998). Disequilibrium during metamorphism: The role of nucleation kinetics. In P. J. Treloar & P. J. O'Brien (Eds.), *What drives metamorphism and metamorphic reactions? Geological Society of London Special Publication*, *138*, 199–214.

Spear, F. S. (1993). Metamorphic phase equilibria and pressure–temperature–time paths. *Mineralogical Society of America Monograph*, *1*, 799 pp.

Spear, F. S. (2014). The duration of near-peak metamorphism from diffusion modelling of garnet zoning. *Journal of Metamorphic Geology*, *32*(8), 903–914. https://doi.org/10.1111/jmg.12099

Spear, F. S., & Cheney, J. T. (1989). A petrogenetic grid for pelitic schists in the system SiO_2-Al_2O_3-FeO-MgO-K_2O-H_2O. *Contributions to Mineralogy and Petrology*, *101*, 149–164. https://doi.org/10.1007/BF00375302

Spear, F. S., & Pattison, D. R. M. (2017). The implications of overstepping for metamorphic assemblage diagrams (MADs). *Chemical Geology*, *457*, 38–46. https://doi.org/10.1016/j.chemgeo.2017.03.011

Spear, F. S., & Rumble, D. (1986). Pressure, temperature, and structural evolution of the Orfordville belt, west-central New-Hampshire. *Journal of Petrology*, *27*, 1071–1093. https://doi.org/10.1093/petrology/27.5.1071

Thompson, J. B. (1972). Oxides and sulfides in regional metamorphism of pelitic schists. 24th International Geological Congress (24th Session, Montreal) Report, Section 10, 27–35.

Thompson, A. B. (1976). Mineral reactions in pelitic rocks: I. Prediction of P-T-X(Fe-Mg) phase relations. II. Calculation of some P–T-X(Fe-Mg) phase relations. *American Journal of Science*, *276* (401–424), 425–454. https://doi.org/10.2475/ajs.276.4.425

Thompson, J. B., & Norton, S. A. (1968). Paleozoic regional metamorphism in New England and adjacent areas. In E-an Zen, W. S. White, J. B. Hadley, & J. B. Thompson (Eds.), *Studies of Appalachian geology – Northern and maritime* (pp. 319–327). New York, NY: John Wiley and Sons.

Tinkham, D. K., & Ghent, E. D. (2005). Estimating P-T conditions of garnet growth with isochemical phase diagram sections and the problem of effective bulk-composition. *Canadian Mineralogist*, *43*, 35–50. https://doi.org/10.2113/gscanmin.43.1.35

Tinkham, D. K., Zuluaga, C. A., & Stowell, H. H. (2001). Metapelite phase equilibria modeling in MnNCKFMASH: The effect of variable Al_2O_3 and MgO/(MgO+FeO) on mineral stability. *Mineralogical Society of America: Geological Materials Research*, *3*, 1–42.

Vernon, R. H. (1979). Formation of late sillimanite by hydrogen metasomatism (base-leaching) in some high-grade gneisses. *Lithos*, *12*, 143–152. https://doi.org/10.1016/0024-4937(79)90045-8

Viete, D. R., Hermann, J., Lister, G., & Stenhouse, I. (2011). The nature and origin of the Barrovian metamorphism, Scotland: Diffusion length scales in garnet and inferred thermal time scales. *Journal of the Geological Society*, *168*, 115–132. https://doi.org/10.1144/0016-76492009-087

Viete, D. R., Oliver, J. H., Fraser, G. L., Forster, M. A., & Lister, G. S. (2013). Timing and heat sources for the Barrovian metamorphism, Scotland. *Lithos*, *177*, 148–163. https://doi.org/10.1016/j.lithos.2013.06.009

Waters, D. J., & Lovegrove, D. P. (2002). Assessing the extent of disequilibrium and overstepping of prograde metamorphic reactions in metapelites from the Bushveld Complex aureole, South Africa. *Journal of Metamorphic Geology*, *20*, 135–149. https://doi.org/10.1046/j.0263-4929.2001.00350.x

Webster, E. R., & Pattison, D. R. M. (2018). Polyphase metamorphism and deformation in the southern Omineca belt, southeastern British Columbia. *Canadian Journal of Earth Sciences*, *55*, 84–110. https://doi.org/10.1139/cjes-2017-0036

Weiss, S. (2014). Disthen von der Alpe Sponda, Tessin, Schweiz. *Lapis*, *39*, 12–25.

Wenk, H. R. (1980). Defects along kyanite-staurolite interfaces. *American Mineralogist*, *65*, 766–769.

White, R. W., Pomroy, N. E., & Powell, R. (2005). An in-situ metatexite–diatexite transition in upper amphibolite facies rocks from Broken Hill, Australia. *Journal of Metamorphic Geology*, *23*, 579–602. https://doi.org/10.1111/j.1525-1314.2005.00597.x

White, R. W., Powell, R., & Holland, T. J. B. (2007). Progress relating to calculation of partial melting equilibria for metapelites. *Journal of Metamorphic Geology*, *25*, 511–527. https://doi.org/10.1111/j.1525-1314.2007.00711.x

White, R. W., Powell, R., Holland, T. J. B., Johnson, T. E., & Green, C. R. (2014). New mineral activity–composition relations for thermodynamic calculations in metapelitic systems. *Journal of Metamorphic Geology*, *32*, 261–286. https://doi.org/10.1111/jmg.12071

White, R. W., Powell, R., & Johnson, T. E. (2014). The effect of Mn on mineral stability in metapelites revisited: New a–x relations for manganese-bearing minerals. *Journal of Metamorphic Geology*, *32*, 809–828. https://doi.org/10.1111/jmg.12095

Whitney, D. L., Mechum, T. A., Kuehner, S. M., & Dilek, Y. R. (1996). Progressive metamorphism of pelitic rocks from protolith to granulite facies, Dutchess County, New York, USA: Constraints on the timing of fluid infiltration during regional metamorphism. *Journal of Metamorphic Geology*, *14*, 163–181. https://doi.org/10.1046/j.1525-1314.1996.05836.x

Yardley, B. W. D. (1977). The nature and significance of the mechanisms of sillimanite growth in the Connemara schists, Ireland. *Contributions to Mineralogy and Petrology*, *65*, 53–58. https://doi.org/10.1007/BF00373570

Yardley, B. W. D., Leake, B. E., & Farrow, C. M. (1980). The metamorphism of Fe-rich pelites from Connemara, Ireland. *Journal of Petrology*, *21*, 365–399. https://doi.org/10.1093/petrology/21.2.365

Zaleski, E., Froese, E., & Gordon, T. M. (1991). Metamorphic petrology of Fe-Zn-Mg-Al alteration at the Linda volcanogenic massive sulfide deposit, Snow Lake, Manitoba. *Canadian Mineralogist*, *29*, 995–1017.

How to cite this article: Pattison DRM, Spear FS. Kinetic control of staurolite–Al_2SiO_5 mineral assemblages: Implications for Barrovian and Buchan metamorphism. *J Metamorph Geol*. 2018;36:667–690. https://doi.org/10.1111/jmg.12302